Journal for ImmunoTherapy of Cancer

WDR5-H3K4me3 epigenetic axis regulates OPN expression to compensate PD-L1 function to promote pancreatic cancer immune escape

Chunwan Lu,[1] Zhuoqi Liu,[2] John D Klement,[3,4,5] Dafeng Yang,[3,4,5] Alyssa D Merting,[3,4,5] Dakota Poschel,[3,4,5] Thomas Albers,[4] Jennifer L Waller,[6] Huidong Shi,[4] Kebin Liu [3,4,5]

To cite: Lu C, Liu Z, Klement JD, *et al*. WDR5-H3K4me3 epigenetic axis regulates OPN expression to compensate PD-L1 function to promote pancreatic cancer immune escape. *Journal for ImmunoTherapy of Cancer* 2021;**9**:e002624. doi:10.1136/jitc-2021-002624

► Additional online supplemental material is published online only. To view, please visit the journal online (http://dx.doi.org/10.1136/jitc-2021-002624).

Accepted 29 June 2021

For numbered affiliations see end of article.

Correspondence to
Dr Kebin Liu; kliu@augusta.edu

Dr Chunwan Lu; Chunwanlu@tju.edu.cn

ABSTRACT

Background Despite PD-L1 (Programmed death receptor ligand-1) expression on tumor cells and cytotoxic T lymphocytes tumor infiltration in the tumor microenvironment, human pancreatic cancer stands out as one of the human cancers that does not respond to immune checkpoint inhibitor (ICI) immunotherapy. Epigenome dysregulation has emerged as a major mechanism in T cell exhaustion and non-response to ICI immunotherapy, we, therefore, aimed at testing the hypothesis that an epigenetic mechanism compensates PD-L1 function to render pancreatic cancer non-response to ICI immunotherapy.

Methods Two orthotopic pancreatic tumor mouse models were used for chromatin immunoprecipitation-Seq and RNA-Seq to identify genome-wide dysregulation of H3K4me3 and gene expression. Human pancreatic tumor and serum were analyzed for osteopontin (OPN) protein level and for correlation with patient prognosis. OPN and PD-L1 cellular location were determined in the tumors using flow cytometry. The function of WDR5-H3K4me3 axis in OPN expression were determined by Western blotting. The function of H3K4me3-OPN axis in pancreatic cancer immune escape and response to ICI immunotherapy was determined in an orthotopic pancreatic tumor mouse model.

Results Mouse pancreatic tumors have a genome-wide increase in H3K4me3 deposition as compared with normal pancreas. OPN and its receptor CD44 were identified being upregulated in pancreatic tumors by their promoter H3K4me3 deposition. OPN protein is increased in both tumor cells and tumor-infiltrating immune cells in human pancreatic carcinoma and is inversely correlated with pancreatic cancer patient survival. OPN is primarily expressed in tumor cells and monocytic myeloid-derived suppressor cells (M-MDSCs), whereas PD-L1 is expressed in tumor cells, M-MDSCs, polymorphonuclear MDSCs and tumor-associated macrophages. WDR5 is essential for H3K4me3-specific histone methyltransferase activity that regulates OPN expression in tumor cells and MDSCs. Inhibition of WDR5 significantly decreased OPN protein level. Inhibition of WDR5 or knocking out of OPN suppressed orthotopic mouse pancreatic tumor growth. Inhibition of WDR5 also significantly increased efficacy of anti-PD-1 immunotherapy in suppression of mouse pancreatic tumor growth in vivo.

Conclusions OPN compensates PD-L1 function to promote pancreatic cancer immune escape. Pharmacological inhibition of the WDR5-H3K4me3 epigenetic axis is effective in suppressing pancreatic tumor immune escape and in improving efficacy of anti-PD-1 immunotherapy in pancreatic cancer.

BACKGROUND

Immune checkpoint inhibitor (ICI) immunotherapy has made breakthroughs in many human cancers.[1] However, pancreatic cancer is refractory to ICI immunotherapy.[2–4] Only patients with the mismatch repair deficiency pancreatic cancer, which account for about 0.8% of all human pancreatic cancer cases, have an objective response to ICI immunotherapy.[5–7] The lack of response of human pancreatic cancer to ICI immunotherapy has been linked to the low tumor mutation burden (TMB). Human pancreatic tumor has a median mutational load of 4, much lower than the more immunogenic melanoma and lung cancer.[8] However, despite the low TMB, human pancreatic carcinoma has a low to moderate level of cytotoxic T lymphocyte (CTL) tumor infiltration,[9–11] suggesting that the CTL tumor infiltration level may not be a major mechanism underlying pancreatic cancer non-response to ICI immunotherapy. It is possible that functional suppression of the tumor-infiltrating CTLs in the pancreatic tumor microenvironment may underlies pancreatic cancer non-response to ICI immunotherapy,[10 12–14] which raises the possibility that other immune checkpoints and/or immune suppressive mechanisms compensate PD-L1 function to render pancreatic cancer non-response to ICI immunotherapy,[15–17] which remains to be determined.

In the tumor microenvironment, T cells become dysfunctional and eventually acquire

an exhaustion phenotype usually through regulation by exhaustion-specific epigenetic enhancers.[18] A largely underappreciated mechanism that may also contribute to tumor immune escape and non-response to ICI immunotherapy in pancreatic cancer is the dysregulation of epigenome in the tumor cells.[19–21] H3K4me3 is known to regulate pancreatic cancer immune suppression and response to therapy.[14 22 23] We aimed at testing the hypothesis that H3K4me3 regulates pancreatic carcinoma epigenome dysfunction to render pancreatic cancer non-response to ICI immunotherapy and performed genome-wide H3K4me3 chromatin immunoprecipitation (ChIP)-Seq of orthotopic pancreatic mouse tumor. To this end, we determined that H3K4me3 deposition is highly enriched through pancreatic tumor genome and identified *Spp1*, the gene that encodes osteopontin (OPN) protein, and its receptors as the targets of H3K4me3 in promotion of pancreatic cancer immune escape and non-response to anti-PD-1 immunotherapy.

METHODS

Human pancreatic cancer patient specimens

The non-neoplastic human pancreas and human pancreatic tumor tissues were obtained from the Cooperative Human Tissue Network Southern Division (University of Alabama at Birmingham, AL) (online supplemental tables 1 and 2). Serum specimens of healthy donors and human pancreatic cancer patients were provided by Georgia Cancer Center Biorepository.

Patient dataset analysis

OPN mRNA datasets of non-neoplastic human pancreas and human pancreatic tumor were extracted from TCGA database. For determination of patient survival time correlation with OPN expression level, TCGA pancreatic cancer patient survival and OPN expression datasets were extracted from OncoLnc database. The Kaplan-Meier survival curves were generated from the datasets with a cutoff-high 60% (n=105) and cutoff-low 40% (n=70) using the website's default program. The significance was determined by log rank p value. The patient survival and OPN expression data are presented in online supplemental table 3.

Mice

Female and male C57BL/6 mice were purchased from the Jackson Laboratory (Bar Harbor, Maine, USA). All mice used in this study were between 2 and 3 months old at the start of the experiment.

Cell lines

The mouse pancreatic tumor UN-KC-6141 cell line was provided by Surinder K Batra at the University of Nebraska Medical Center (Omaha, NE). UN-KC-6141 cell line was characterized previously.[24] PANC02-H7 cells were provided by Dr. Min Li at the University of Oklahoma Health Sciences Center (Oklahoma City, OK). PANC02-H7 cell line were characterized previously.[25] J774M cells were sorted from J774 parent cells for $CD11b^{+}Gr1^{+}$ cells and characterized as previously described.[26] Cell lines were tested bimonthly for mycoplasma contamination and are mycoplasma-free at the time of use.

The orthotopic pancreatic cancer mouse models

PANC02-H7 and UN-KC-6141 cells (1×10^{4} cells/mouse) were surgically injected to the pancreas of C57BL/6 mice as previously described.[10]

Compound synthesis

WDR5-47 and WDR5-0102 were synthesized and characterized as previously described.[27] Cpd23 was synthesized and characterized as previously described.[28] In short, for the synthesis of WDR-47 and WDR5-0102, 2-amino-4-nitrofluorobenzene was reacted with the requisite benzoyl chloride in dichloromethane in the presence of pyridine, and the amide thus obtained was then reacted with N-methylpiperidine in DMF (dimethylformamide) in presence of anhydrous potassium carbonate. To synthesize Cpd23, 2-nitro-4-bromofluorobenzene was first reacted with N-methylpiperidine in DMF in presence of anhydrous potassium carbonate and the nitro group then converted to the amine by catalytic hydrogenation. The aromatic amine was then reacted with the appropriate substituted benzoyl chloride in dichloromethane in presence of pyridine. The aromatic bromide was finally coupled with four pyridylboronic acid in dioxane using Pd(PPh3)2Cl2 catalyst and cesium carbonate base. The purity of the compounds is determined by 1H-NMR spectroscopy as >98%. All three compounds were then validated for activity in inhibition of histone methyltransferase activity inhibition in Reaction Biology Corp (Malvern, Pennsylvania, USA).

Histone methyltransferase activity assay

Inhibition of MLL1 enzymatic activity by WDR5-47, WDR5-0102 and Cpd23 was determined in a 10-dose IC_{50} mode with 3-fold serial dilution starting at 10 µM with HotSpot format at Reaction Biology Corp. MLL1-WDR5 protein complexes and nucleosome were used. Reactions were initiated by the addition of ^{3}H-S-adenosyl-methionine (1 µM).

OPN knockout tumor cell line generation and mouse tumor model

HEK293FT cells were cotransfected with pCMV-VSV-G (Addgene #8454), psPAX2 (Addgene #12260) and lentiCRISPRv2 (Genscript, Piscataway, NJ) plasmids containing scramble (GGAAGACTTAGTCGAATGAT) or *Spp1*-specific (GCAAATCACTGCCAATCTCA) sgRNA-coding sequence using Lipofectamine 2000 (Life Technologies) to produce CRISPR lentivirus.[29] PANC02-H7 cells were transduced with the lentivirus particle. Cells were selected with puromycin to generate stable cell lines PANC02-H7.Scramble and PANC02-H7.Spp1 KO, respectively. Cells were cultured in 24-well plate (2.5×10^{5} cells/well in 1 mL medium) for 24 hours. Culture

supernatants were collected for OPN protein measurement by ELISA as described below. PANC02-H7.Scramble and PANC02-H7.Spp1 KO cells (2×10^4 cells/mouse) were surgically injected to pancreas of C57BL/6 mice as previously described.[10] The tumor-bearing mice were treated 5 days after tumor cell injection with IgG or anti-PD-1 (clone RMP1-14, 200 µg/mouse, Bio X Cell, Lebanon, New Hampshire, USA) every 2 days via i.p. injection. Mice were sacrifice 20 days after tumor cell injection to analyze tumor.

OPN protein analysis by ELISA

Human serum was analyzed for OPN protein level using the human OPN ELISA kit (Cat# DOST00, R&D Systems, Minneapolis, MN) according to the manufacturer's instructions. Tumor cell culture supernatant and mouse serum was analyzed for OPN protein level using the mouse OPN ELISA kit (Cat # DY441, R&D System) according to the manufacturer's instructions.

WDR5 therapy and anti-PD-1 immunotherapy

The orthotopic PANC02-H7 tumor-bearing mice were treated 5 days after tumor cell injection. The treatment groups include: solvent control (n=8), WDR5-47 (60 mg/kg body weight in PEG300), anti-PD-1 (clone RMP1-14, 200 µg/mouse). WDR5-47 was administered daily via i.p. injection. Anti-PD-1 was administered every 2 days via i.p. injection. Mice were sacrifice 20 days after tumor cell injection to analyze tumor.

Immunohistochemistry

Tissue sections were stained as previously described.[14] The sections were stained with anti-human OPN antibody (Cat # AF1433. R&D System) and mounted in Vecta-Mount Permanent Mounting Medium (Vector Lab, Burlingame, California, USA).

Chromatin immunoprecipitation

Tumor tissues were collected from orthotopic PANC02-H7 and UN-KC-6141 tumor-bearing mice. Normal whols pancreas were dissected from tumor-free C57BL/6 mice. The normal pancreas and tumor tissues were rinsed in PBS and used immediately for chromatin preparation using the SimpleChIP Plus Enzymatic Chromatin IP Kit (Cat# 9004. Cell Signaling Tech, Danvers, MA). ChIP was performed using anti-H3K4me3 (Cat# 9751. Cell Signaling Tech) and the SimpleChIP Plus Enzymatic Chromatin IP Kit according to the manufacturer's instructions. The immunoprecipitated genomic DNA fragments were analyzed qPCR using PCR primers covering the region of *Spp1* promoter regions (online supplemental table 4).

ChIP-Sequencing

Chromatin fragments were prepared from pancreas of tumor-free C57BL/6 mice and tumors and immunoprecipitated as described above and used to construct the DNA library for next-generation sequencing (NGS) by NGS service provider Novogene Corp (Chula Vista, CA). The quality of raw sequencing reads was examined by FastQC and the adaptor and low quality sequences were trimmed and clean by Trim Galore. The cleaned reads were mapped to mouse reference genome (mm10) using Bowtie2. PCR duplicates were identified and removed by Picard tool. H3K4me3 enriched peaks were identified by MACS2 and annotated using ChIPseeker. Differential peaks between orthotopic pancreatic tumor and normal pancreas were identified by DiffBind. The analysis described above were performed in Galaxy server (use.galaxy.org). The entire dataset is deposited in GEO database (Accession # GSE178677).

Flow cytometry

Tumor tissues were collected and digested in collagenase solution (1 mg/mL collagenase, 0.1 mg/mL hyaluronidase, and 30 U/mL DNase I) and passed through a 100 µm cell filter. Cells were then lysed with red cell lysis buffer, stained with fluorescent dye-conjugated antibodies (online supplemental table 5) and analyzed in a LSRFortessa. All flow cytometry data were analyzed using FlowJo program.

Gene expression analysis

RNA was isolated from tissues using GeneJET RNA Purification Kit (Cat# K0732. Thermo Fisher Scientific) according to manufacturer's instructions. cDNA was synthesized from total RNA and used for analysis of gene expression by qPCR using gene-specific primers (online supplemental table 4) in a StepOne Plus Real-Time PCR System (Applied Biosystems, Foster City, California, USA).

RNA sequencing

Tumor tissues were collected from orthotopic PANC02-H7 and UN-KC-6141 tumor-bearing mice. Normal pancreas were dissected from tumor-free C57BL/6 mice. The normal pancreas and tumor tissues were rinsed in PBS and used for total RNA isolation using the GenJet RNA Isolation Kit (ThermalFisher Scientific). Total RNA was used to construct the cDNA library for high throughout DNA sequencing by Novogene. The cleaned reads were mapped to reference genome (mm10) using STAR aligner. The sequence counts for each gene were collected by featureCounts and annotated using annotateMyIDs function. The differential expression analysis between tumor and normal samples was performed using DESeq2. The above-mentioned analysis were performed in Galaxy server (use.galaxy.org). The heatmaps were generated using ComplexHeatmap in R V.3.6.3. KEGG pathway enrichment analysis was performed using clusterProfiler. The entire dataset is deposited in GEO database (Accession # GSE178677).

Western blotting analysis

Cells were cultured in the presence of various concentrations of WDR5-47, WDR5-0102 and Cpd23 for 24 hours. Cells were then lysed, blotted, and probed with anti-mouse OPN antibody (Cat# AF808, R&D Systems and

Cat#691302, Biolegend) using procedures as previously described.[26]

Cell viability assay

Cell viability assays were performed using CellTiter 96 Aqueous One Solution Cell Proliferation Assay Kit (Cat# G3582, Promega, Madison WI) according to the manufacturer's instructions.

Statistical analysis

A two-factor analysis of variance was used to examine whether there was a synergistic effect of WDR5-47 and OPN (WDR5-47/Control or Scramble/Spp1 KO) with anti-PD-1 immunotherapy (anti-PD-1 vs control) for tumor growth control (tumor size and weight). Each model contained fixed effects of WDR5-47 and OPN, anti-PD-1 status, and the two-factor interaction between these two effects. Of statistical interest was the F-test for the two-factor interaction between WDR5-47/OPN and anti-PD-1. If this F-test is statistically significant, this will indicate that a synergistic effect is evident. A Tukey-Kramer multiple comparison procedure was used to examine post hoc pairwise differences between groups.

RESULTS

The expression of *Spp1* is activated by its promoter H3K4me3 deposition in pancreatic carcinoma in vivo

To profile H3K4me3 deposition change in pancreatic carcinoma genome, we surgically transplanted UN-KC-6141 and PANC02-H7 cells to mouse pancreas to establish orthotopic pancreatic tumor mouse models (figure 1A). Pancreas of UN-KC-6141 and PANC02-H7 tumors were collected and subjected to ChIP and high throughout sequencing. H3K4me3 deposition is enriched throughout the entire genome in both UN-KC-6141 and PANC02-H7 tumors as compared with the normal pancreas (figure 1B,C). As expected, the promoter region of *Cd274*, the gene encoding PD-L1, has increased H3K4me3 deposition (figure 1B,C). Of interest is the finding that *Spp1* and its receptor *Cd44* have increased H3K4me3 deposition in their promoter regions (figure 1B). H3K4me3 deposition is enriched in a region flanking the *Spp1* transcription start site (figure 1D). Individual ChIP analysis validated that H3K4me3 is enriched around the *Spp1* transcription start site in mouse pancreatic carcinoma in vivo (figure 1E).

Consistent with increased H3K4me3 deposition, RNA-Seq analysis determined that *Spp1* and *Cd44* expression levels are increased in both UN-KC-6141 and PANC02-H7 tumors (figure 2A). Increased Spp1 and Cd44 expression in both pancreatic mouse tumor was validated by qPCR analysis (figure 2B,C). Pathway analysis revealed multiple pathways, including PI3K-Akt, MAPK signaling, proteoglycans in cancer, focal adhesion, phagosome, pancreatic secretion, ECM (Extracellular matrix)-receptor interaction, gap junction are enriched in the tumors (online supplemental figure 1). Among these enriched pathways, PI3K-Akt pathway has a large set of genes with increased expression (online supplemental figure 2). *Spp1 and Cd44* are enriched in the ECM-receptor and focal adhesion pathways (online supplemental figure 2). Furthermore, several integrins that function as OPN receptors are also enriched in the ECM-receptor pathways in both tumors in vivo (online supplemental figure 3).

OPN protein is increased in human pancreatic cancer patients and is correlated with poor patient prognosis

To determine the human relevance of the above finding, we analyzed OPN protein level in no-neoplastic human pancreas and pancreatic tumors. OPN protein level is higher in pancreatic tumors than in non-neoplastic pancreas in all five pancreatic patients analyzed (figure 3A–C). Analysis of OPN mRNA datasets from TCGA (The Cancer Genome Atlas) database also determined that OPN expression level is significantly higher in human pancreatic tumor than in normal pancreas (figure 3D). OPN exists as a secreted protein, analysis of serum OPN determined that OPN protein level is significantly higher in serum from pancreatic cancer patients as compared with serum from healthy donors (figure 3E). Furthermore, OPN expression level is inversely correlated with pancreatic cancer patient survival time (figure 3F).

OPN is expressed in monocytic myeloid-derived suppressor cells in pancreatic tumor microenvironment

OPN protein is present in both tumor cells and tumor-infiltrating immune cells in human pancreatic carcinoma (figure 3A). Myeloid cells are major populations of immune cells in pancreatic carcinoma that act as potent immune suppressors. We then sought to determine OPN expression profiles in tumor-infiltrating myeloid cells. A subset of $CD11b^{+}Gr1^{+}$ myeloid-derived suppressor cells (MDSCs) are OPN^{+} in both UN-KC-6141 and PANC02-H7 tumors (figure 4B,C). Further analysis of MDSCs into monocytic MDSCs (M-MDSCs) and polymorphonuclear MDSCs (PMN-MDSCs) indicates that tumor-infiltrating OPN^{+} MDSCs are primarily M-MDSCs in both UN-KC-6141 and PANC02-H7 tumors in vivo (figure 4B,C).

PD-L1 is expressed in PMN-MDSCs and tumor-associated macrophage

We next sought to determine PD-1 and PD-L1 expression profiles in pancreatic tumor. $CD4^{+}$ and $CD8^{+}$ T cells are present in both UN-KC-6141 and PANC02-H7 tumors (figure 5A–C, 5G-I). Approximately 39%–49% tumor-infiltrating $CD4^{+}$ T cells are $PD\text{-}1^{+}$ and 50%–61% $CD8^{+}$ T cells express PD-1 (figure 5D,J). More than 50% tumor-infiltrating MDSCs express PD-L1. About 41%–44% M-MDSCs express PD-L1 and almost all PMN-MDSCs are $PD\text{-}L1^{+}$ (figure 5E,F,K,L). About 83%–93% of tumor-associated macrophages are $PD\text{-}L1^{+}$ cells (figure 5E,F,K,L). Furthermore, all pancreatic tumor cells express high level of PD-L1 in vivo (figure 5E,F,K,L).

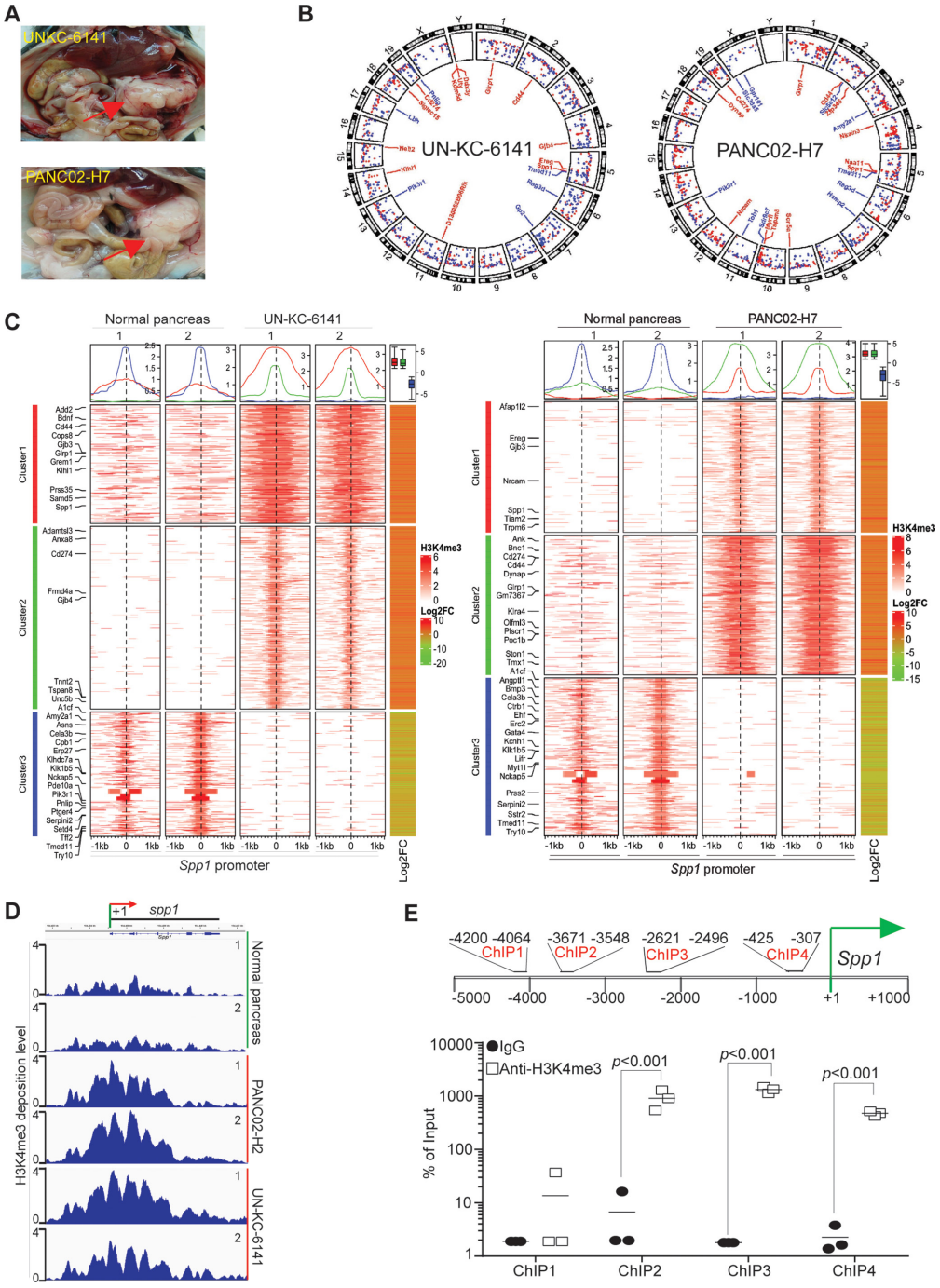

Figure 1 The promoter of *Spp1* and *Cd44* are enriched with H3K4me3 deposition in mouse pancreatic carcinoma in vivo. (A) Orthotopic pancreatic UN-KC-6141 and PANC02-H7 tumor mouse models. the red arrows indicate the tumors. (B) Normal pancreas and the orthotopic pancreatic tumors as shown in A were collected for chromatin preparation and immunoprecipitation using H3K4me3-specific antibody. The CHIP DNA libraries were sequenced by illumina NGS sequencing and analyzed using bioinformatics pipeline described in the methods. Shown is the circos plot of the genome-wide distribution of differential H3K4me3 peaks between normal and tumor samples along all chromosomes. The differential peaks with log2 fold change >1 are shown and peaks associated several genes with known functions in immune suppression and tumor progression are mapped in the inner circle. (C) The left two heatmaps illustrate differential H3K4me3 signals within the 2 kb window from the center of each peak. The H3K4me3 ChIP-Seq data from two biological replicates were merged and used to plot the heatmap. The line graphs on top of the heatmap demonstrate the average accessibility profiles of three clusters with increased or decreased H3K4me3 signals. The column on the right which shows matched average expression log2FC of 2 replicates, and the results are summarized in the box plot shown on top of the column. Representative genes with significant changes in both H3K4me3 and gene expression are listed beside the heatmap. (D) H3K4me3 deposition profile in the *Spp1* gene region. (E) *Spp1* promoter structure showing CHIP PCR-amplified regions (top panel). UN-KC-6141 tumors were analyzed by H3K4me3 CHIP and qPCR (bottom panel) using the PCR primer pairs as indicated in the top panel ChIP-Seq, chromatin immunoprecipitation sequencing.

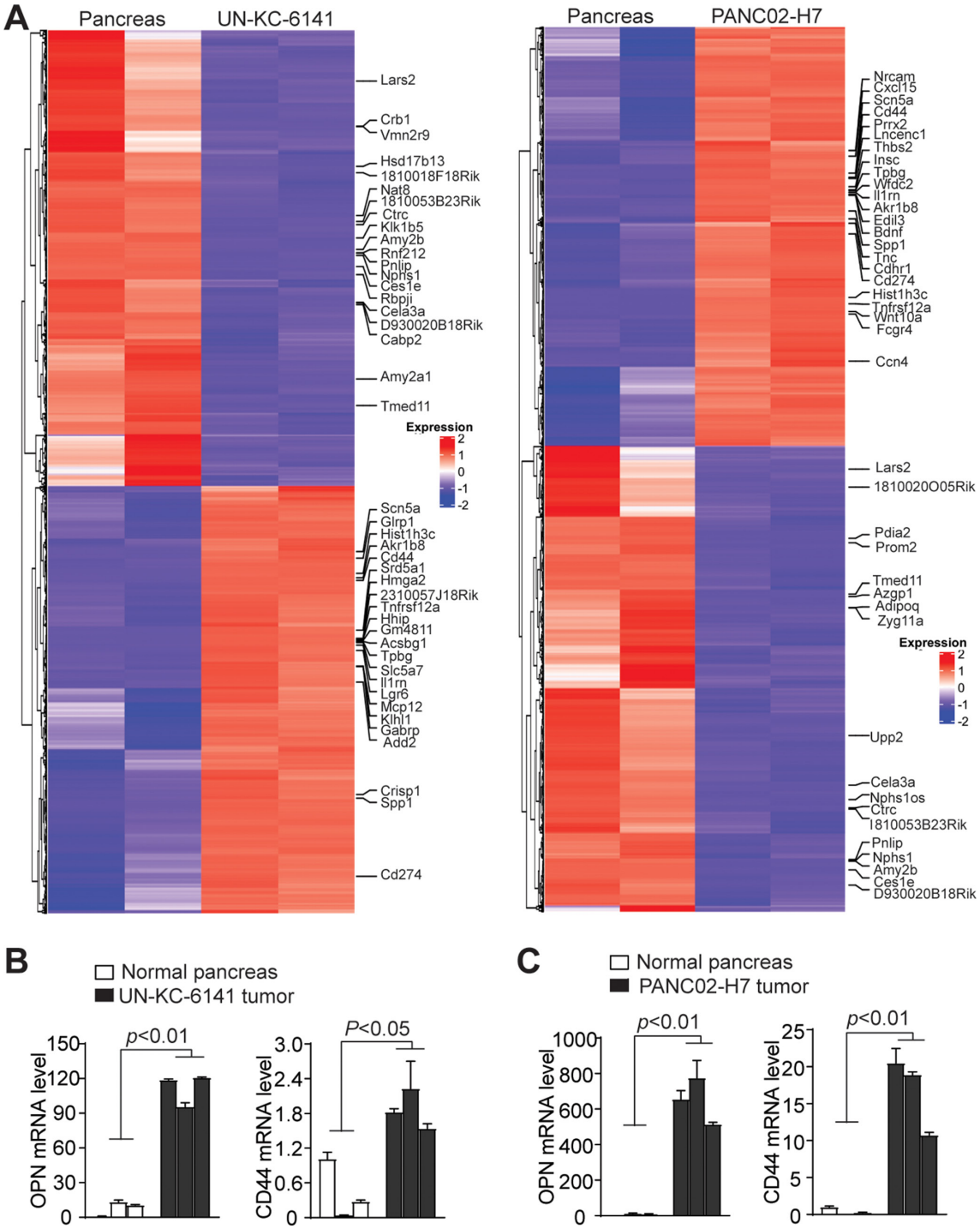

Figure 2 Transcriptome analysis of mouse pancreatic tumor in vivo. (A) RNA was extracted from normal pancreas and the orthotopic mouse pancreatic tumors as shown in figure 1A and analyzed by RNA-seq. Differentially expressed genes were extracted and displayed in heatmap. The gene expression level was displayed in color gradient as indicated in the right. Several genes with known functions in immune suppression and tumor progression are indicated at the right. (B, C) qPCR analysis of OPN and CD44 expression in normal pancreas as compared with UN-KC-6141 (B) and PANC02-H7 (C) tumors. Each column indicates data from one mouse. OPN, osteopontin.

The WDR5-H3K4me3 epigenetic axis regulates OPN expression in pancreatic tumor cells and MDSCs

The mixed lineage leukemia family of proteins (Mll1-4/Kmt2a-d, SET1A and SET1B, Set1, and Smyd) selectively methylate histone 3 Lys4 (H3K4). The enzyme activity of these histone methyltransferases requires adaptor proteins WDR5, RBBP5 and ASH2L.[30] Histone methyltransferase Smyd2/Kmt3c has been shown to be up-regulated in pancreatic cancer to render resistance to chemotherapy.[31] RNA-seq analysis revealed a large set of histone lysine methyltransferases, including H3K4me3-selective methyltransferase, are highly upregulated in both

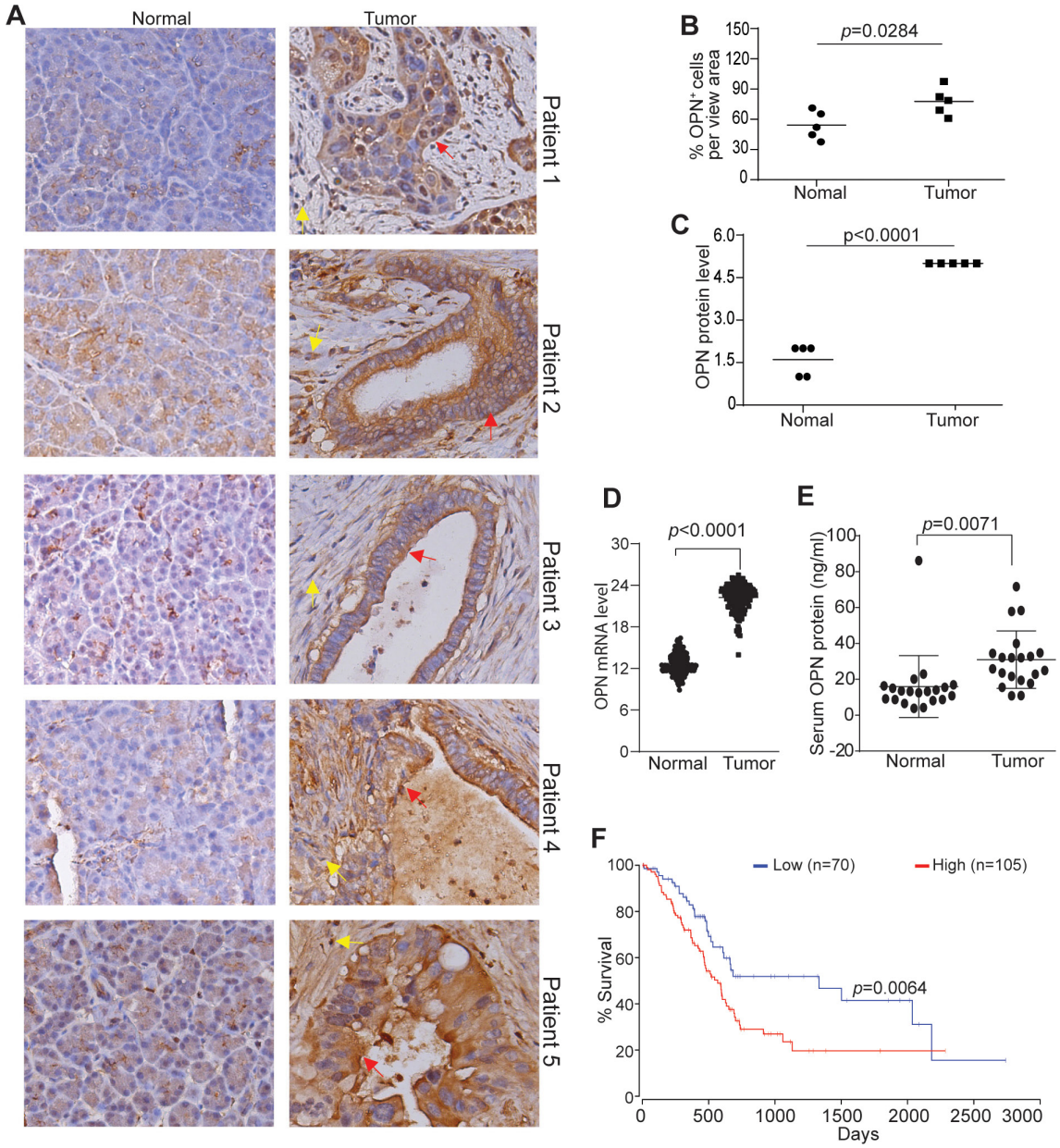

Figure 3 OPN protein level in non-neoplastic human pancreas and human pancreatic carcinoma. (A) Human non-neoplastic pancreas (n=5) and pancreatic tumor (n=5) were stained with OPN-specific antibody. brown color indicates OPN staining intensity. shown are representative images. (B) Quantification of OPN$^+$ cells in the pancreas and pancreatic tumor as shown in A. (C) OPN protein intensity in normal pancreas and pancreatic tumor as shown in A. The relative OPN staining intensity is set at 1–5. (D) OPN mRNA level datasets of non-neoplastic pancreas (n=182) and pancreatic tumor (n=167) were extracted from TCGA database and plotted. (E) Serum specimens were collected from healthy donors (n=20) and pancreatic cancer patients (n=20) and measured for OPN protein level by ELISA. (F) OPN mRNA expression level and pancreatic cancer patient survival datasets were extracted from OncoLnc database. Kaplan-Meier survival curve was generated with a 40% low OPN cut-off and 60% high OPN cut-off using log rank test. OPN, osteopontin.

UN-KC-6141 and PANC02-H7 tumors in vivo as compared with normal pancreas (figure 6A). WDR5 forms a protein complex with these methyltransferases and is essential for enzyme activity of all H3K4me3-specific histone methyltransferases.[27 28] We, therefore, pursued WDR5 inhibition to suppress H3K4me3 in pancreatic tumors. WDR5-47, WDR5-0102, and cpd23 are well-characterized small molecule WDR5 inhibitors for H3K4 trimethylation.[27 28] Analysis of MLL1-WDR5 histone methyltransferase activity in the presence of WDR-47, WDR5-0102, and cpd23 determined that all these three compounds inhibit MLL1-WDR5 enzymatic activity in a dose-dependent manner (figure 6B). We then cultured pancreatic tumor cells in the presence of these inhibitors and analyzed OPN protein level. All these three WDR5-selective inhibitors decrease OPN protein level in pancreatic tumor cells in vitro (figure 6C). WDR5-47 and WDR5-0102 exhibit minimal cytotoxicity to pancreatic tumor cells, whereas

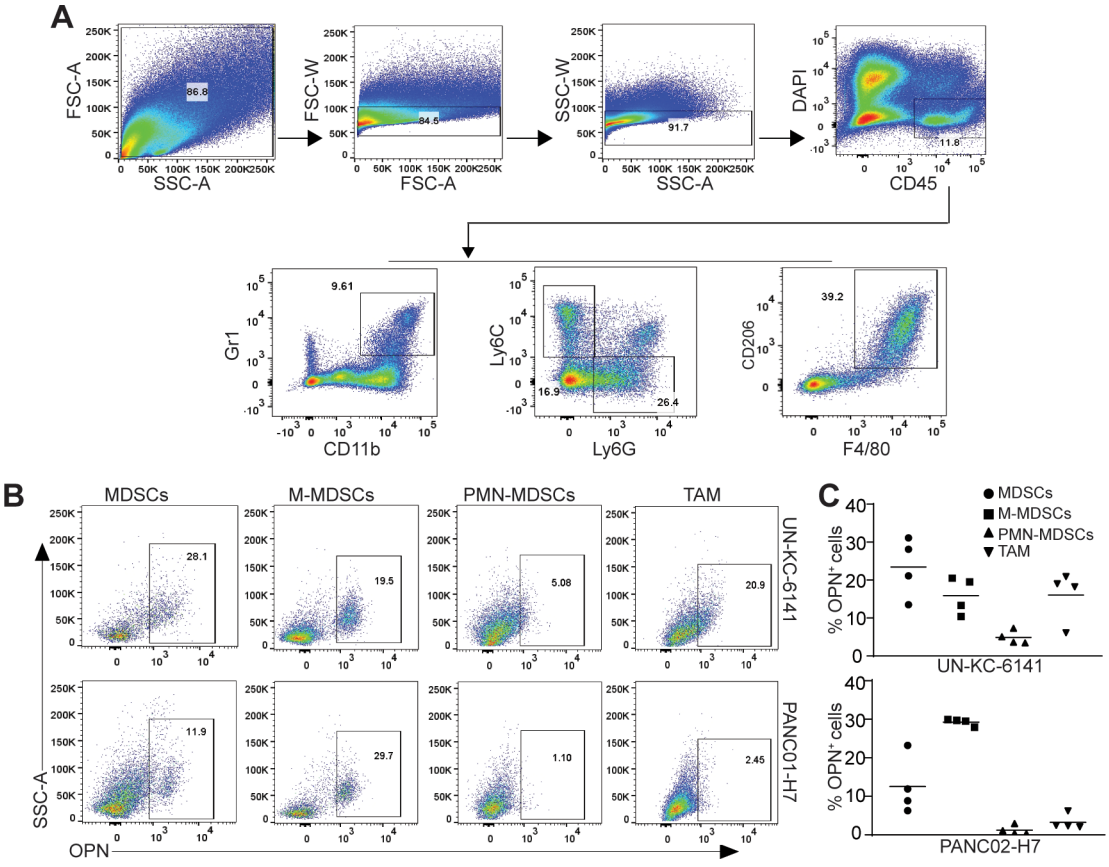

Figure 4 OPN cellular expression profiles in myeloid cells in pancreatic mouse tumors in vivo. (A) UN-KC-6141 and PANC02-H7 tumors were collected, digested with collagenase, stained with the indicated antibodies, and analyzed by flow cytometry. Shown is the gating strategy. (B) Subsets of tumor-infiltrating myeloid cells were analyzed for OPN$^+$ cells in the two mouse tumor models. (C) Quantification of OPN$^+$ subsets of tumor-infiltrating myeloid cells in the two pancreatic tumors. OPN, osteopontin.

cpd23 showed significant cytotoxicity to pancreatic tumor cells (figure 6D). We next sought to determine whether these WDR5-selective inhibitors inhibit OPN expression in MDSCs. J774M is a CD11b$^+$Gr1$^+$ MDSC-like cell line established from the parent J774 monocytic leukemia cell lines. J774M cells have potent inhibitory activity against T cell activation in vitro and thus mimic MDSCs in vitro.[26] We treated J774M cells with these WDR5-selective inhibitors and analyzed OPN protein level. All three inhibitors decrease OPN protein level in J774M cells in a dose-dependent manner (figure 6F). Analysis of cell viability determined that WDR5-47 has no cytotoxicity to J774M, and WDR5-0102 and cpd23 exhibit a dose-dependent cytotoxicity to J774M cells (figure 6E).

Inhibition of WDR5 represses OPN production and enhances efficacy of anti-PD-1 immunotherapy

We then reasoned that targeting pancreatic tumor with a WDR5 inhibitor should be effective in suppression of pancreatic tumor growth in vivo. To test this hypothesis, we made use of the orthotopic pancreatic tumor mouse models. Both UN-KC-6141 and PANC02-H7 tumor-infiltrating T cells express FasL and granzyme B (online supplemental figure 4A-C), two essential effectors of the host T cells.[32] Analysis of tumor cells revealed that PANC02-H7 express the death receptor Fas while UN-KC-6141 tumor cells lack Fas expression on its surface in vivo (online supplemental figure 4D). We therefore made use of PANC02-H7 tumor model in this proof-of-principle study. WDR5-47 was used as the WDR5 inhibitor due to its minimal direct cytotoxicity and low IC_{50}. Tumor-bearing mice were treated with WDR5-47 and anti-PD-1 either alone or in combination. OPN is secreted protein. Consistent with the in vitro observation that WDR5-47 treatment decreases OPN protein level in tumor cells and MDSCs (figure 6C,F). Treatment of tumor-bearing mice with WDR5-47 significantly decreased OPN protein level in the peripheral blood (figure 7A).

Consistent with the decreased OPN protein level by WDR5-47 treatment in tumor-bearing mice, a statistically significant interaction between WDR5-47 and anti-PD-1 was detected for tumor weight ($F(1,28)=6.97$, $p=0.0134$) (online supplemental table 6, figure 7B). The control group had the highest tumor weight, followed by WDR5-47, anti-PD-1 alone, and then WDR5–47+ anti-PD-1 with the lowest tumor weight (online supplemental table 6). The Tukey-Kramer multiple comparison test on the interaction effect indicated that tumor weights were significantly lower for the WDR5–47+ anti-PD1 when compared

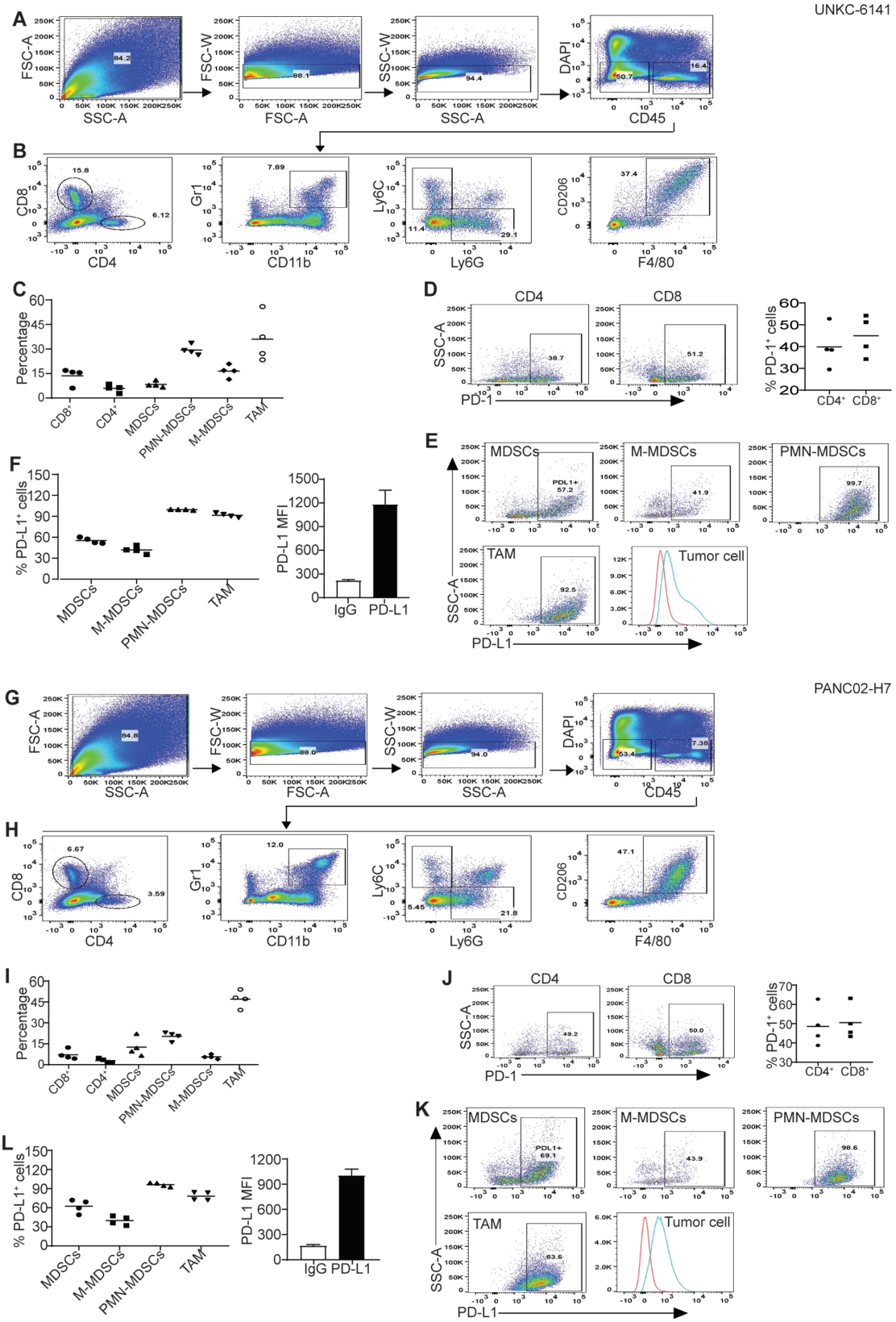

Figure 5 Tumor-infiltrating immune cell profiles and PD-1/PD-L1 cellular profiles in pancreatic mouse tumors in vivo. (A, G) Tumors were collected from UN-KC-6141 (A–F) and PANC02-H7 (G–L) tumor-bearing mice and processed as in figure 4A. Shown is the gating strategy. (B, H) Analysis of tumor-infiltrating T cells and myeloid cells. (C, I) Quantification of T cells and myeloid cell subsets as shown in (B, H). (D, J) PD-1 expression in tumor-infiltrating T cells. (E, K) Analysis of PD-L1 expression in subsets of tumor-infiltrating myeloid cells and tumor cells. (F, L) Quantification of PD-L1$^+$ subsets of tumor-infiltrating myeloid cells (left panel) and PD-L1 MFI in tumor cells (right panel). M-MDSCs, monocytic myeloid-derived suppressor cells; PMN, polymorphonuclear; TAM, tumor-associated macrophage; FSC:forward scatter; SSC: side scatter.

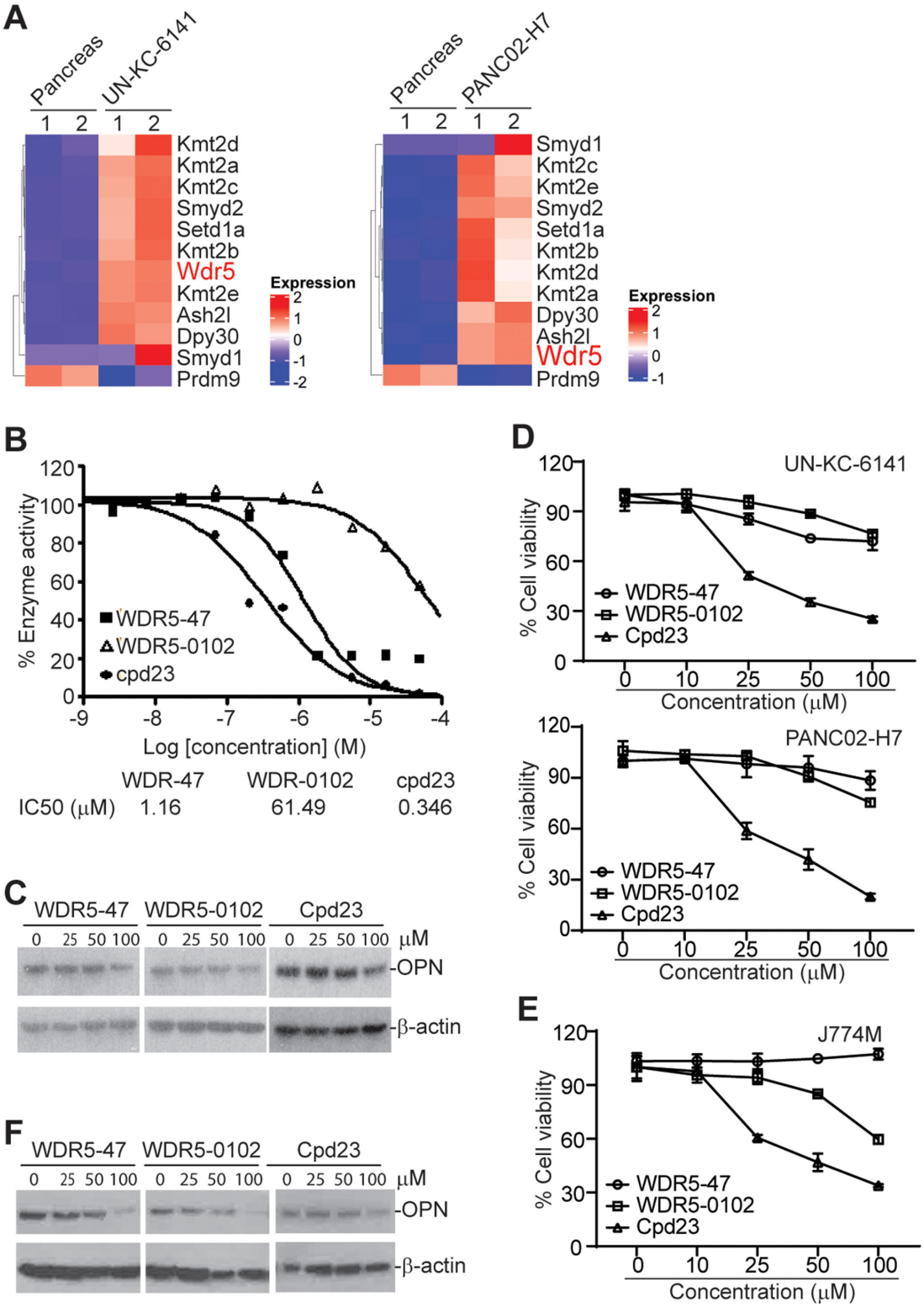

Figure 6 The WDR5-H3K4me3 axis regulates OPN expression in tumor cells and MDSCs. (A) Heatmap of differentially expressed histone methyltransferases. Shown are ratios of tumor versus normal pancreas with red indicates upregulation in tumor cells and blue indicates downregulation in tumor cells. (B) WDR5 inhibitors were tested in a 10-dose IC_{50} mode with threefold serial dilutions using [^{3}H]S-adenosyl-methionine as substrate with recombinant human MLL1-WDR5 complex. The enzyme activity was plotted against inhibitor concentrations. IC_{50}s were calculated using the GraphPad prism program. (C) UN-KC-6141 cells were cultured in the presence of WDR5 inhibitors at the indicated concentrations for 24 hours and analyzed by Western blotting. (D) Tumor cells were cultured in the presence of WDR5 inhibitors at the indicated concentrations for 24 hours and analyzed for cell viability. (E) J774M cells were cultured in the presence of WDR5 inhibitors at the indicated concentrations for 24 hours and analyzed for cell viability. (F) J774M cells were cultured in the presence of WDR5 inhibitors at the indicated concentrations for 24 hours and analyzed by Western Blotting. MDSCs, myeloid-derived suppressor cells; OPN, osteopontin.

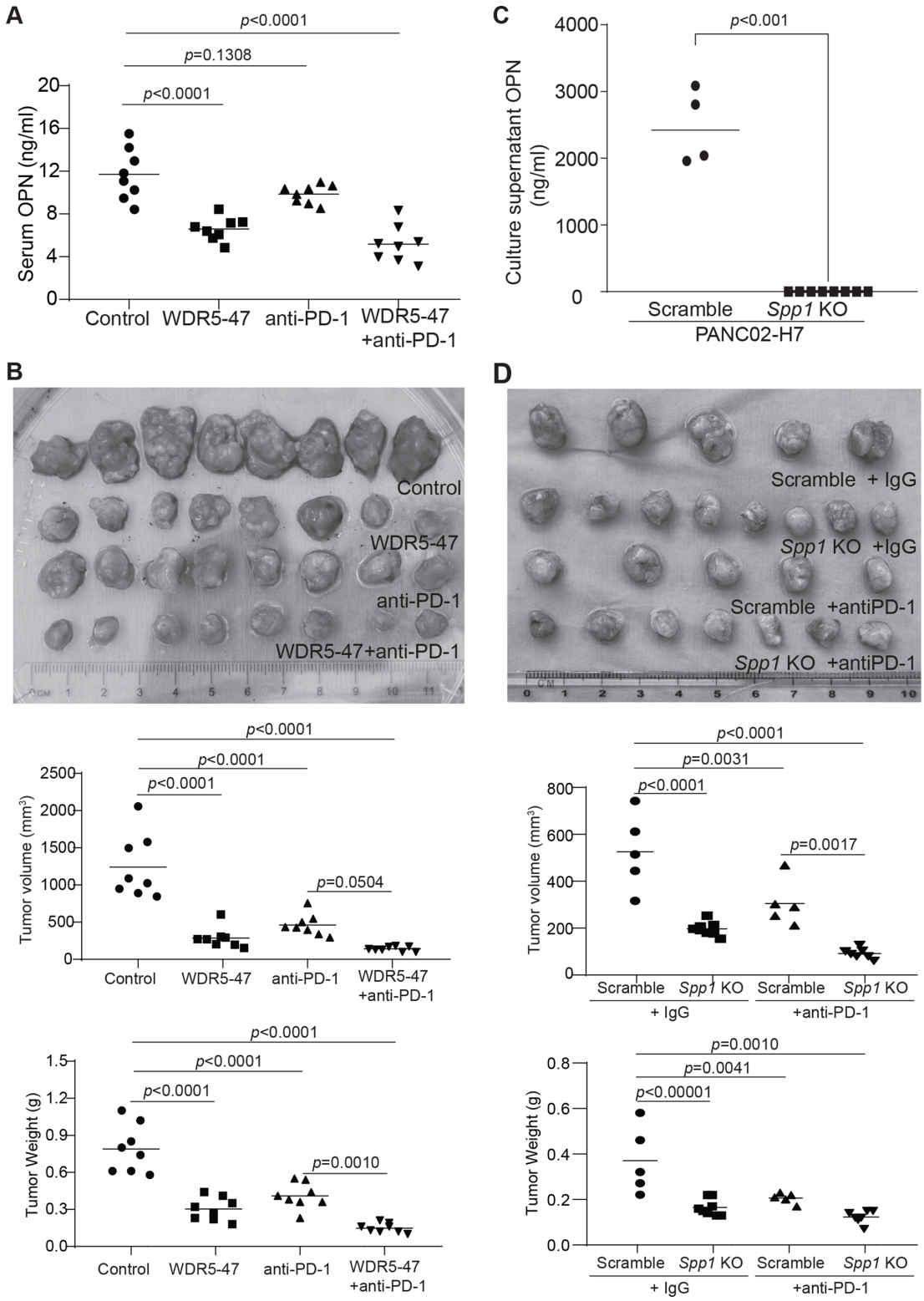

Figure 7 Targeting WDR5 decreases OPN level and increases efficacy of anti-PD-1 immunotherapy in suppression of pancreatic tumor growth in vivo. (A) PANC02-H7 cells (1×10^4 cells/mouse) were surgically transplanted into mouse pancreas. The tumor-bearing mice were treated 5 days later with solvent, WDR5-47 (60 mg/kg body weight) daily, anti-PD-1 every 2 days, or WDR5–47+ anti-PD-1. Mice were sacrificed on day 20. Serum was collected and measured for OPN protein level by ELISA. (B) Tumors were dissected and measured for tumor size and weight. A Tukey-Kramer multiple comparison test was used to determine statistical significance. (C) PANC02-H7.Scramble and PANC02-H7.Spp1 KO cell culture supernatants were analyzed by ELISA for OPN protein concentration. (D) PANC02-H7.Scramble and PANC02-H7.Spp1 KO cells (2×10^4 cells/mouse) were surgically transplanted to mouse pancreas. The tumor-bearing mice were treated 5 days later with IgG and anti-PD-1 (200 µg/mouse) every 2 days. Mice were sacrificed on day 20. Tumors were dissected and measured for tumor size and weight. A Tukey-Kramer multiple comparison test was used to determine statistical significance. KO, knock out; OPN, osteopontin.

with the control (p<0.0001) and anti-PD-1 (p=0.0010). The control group had significantly higher tumor weights than all other groups (p<0.0001 for each comparison to anti-PD-1, WDR5-047, and WDR5+ anti-PD-1). There were no statistically significant differences between anti-PD-1 and WDR-47 (p=0.3161) nor WDR-47 compared with WDR5–47+anti-PD-1 (p=0.0756). A statistically significant interaction between WDR5-47 and anti-PD-1 was also detected for tumor size (F(1,28)=14.29, p=0.0008) (online supplemental table 6, figure 7B). The control group had the largest tumor size, followed by anti-PD-1, WDR5-47, and then WDR5–47+ anti-PD-1 with the smallest tumor size. The Tukey-Kramer multiple comparison test on the interaction effect indicated that the control group had significantly greater tumor size than all other groups (p<0.0001 for each comparison to anti-PD-1, WDR5-47, and WDR5–47+ anti-PD-1. There were no other statistically significant differences between groups (anti-PD-1 vs WDR5-47: p=0.4640; anti-PD-1 vs WDR5–47+anti-PD-1: p=0.0504; WDR5-47 vs anti-PD-1: p=0.6016). Taken together, these findings indicate that combined WDR5-47 and anti-PD-1 therapy has a significantly higher efficacy in suppression of the orthotopic PANC02-H7 tumor growth than either WDR5-47 or anti-PD-1 therapy alone.

H3K4me3 also regulates PD-L1 expression.[14] To determine the direct effect of OPN on pancreatic tumor growth and response to anti-PD-1 immunotherapy, we knocked out *Spp1*, the gene that encodes OPN (figure 7C), in PANC02-H7 cells. ELISA analysis confirmed that *Spp1* is knocked out (figure 7C). PANC02-H7.Scramble and PANC02-H7.Spp1 KO cells were then surgically transplanted to C57BL/6 mice to establish orthotopic tumor. A higher tumor cell dose was used in this model due to the increased immunogenicity of the tumor cells after lentiviral vector transduction. The OPN WT and KO tumor-bearing mice were then treated with anti-PD-1 mAb. A statistically significant interaction between OPN status and anti-PD-1 was detected for tumor weight (F(1,21)=5.28, p=0.0319) (online supplemental table 7, figure 7D). OPN WT (Scramble) had the highest tumor weight, followed by WT +anti-PD1, *Spp1* KO, and then *Spp1* KO +anti-PD1 (the lowest tumor weight). The Tukey-Kramer multiple comparison test on the interaction effect indicated that tumor weights were significantly higher for the WT tumor when compared with all other groups (*Spp1* KO: p<0.0001, *Spp1* KO+ anti-PD1: p=0.0010, WT +anti-PD1: p=0.0041). There were no statistically significant differences between *Spp1* KO and *Spp1* KO+ anti-PD1 (p=0.6576), *Spp1* KO and WT +anti-PD1 (p=0.7371), or *Spp1* KO+ anti-PD1 and WT+ anti-PD1 (p=0.2115).

Unlike the patterns in tumor weight, there was no statistically significant interaction between OPN status and anti-PD-1 in terms of tumor size (online supplemental table 7, figure 7D). However, the Tukey-Kramer multiple comparison test on the interaction effect indicated that WT tumor had significantly higher tumor size when compared with all other groups (*Spp1* KO: p<0.0001, *Spp1* KO+ anti-PD1: p=<0.0001, WT+ anti-PD1: p=0.0031). *Spp1* KO+ anti-PD-1 had significantly lower tumor size when compared with WT+ anti-PD1 (p=0.0017). There were no statistically significant differences in tumor size for *Spp1* KO and *Spp1* KO+ anti-PD1 (p=0.1092) or *Spp1* KO and WT +anti-PD1 (p=0.1478). Taken together, these findings indicate that knocking out OPN significantly reduced both tumor size and weight and there is a statistically significant interaction between OPN status and anti-PD-1 efficacy in terms of tumor weight in tumor-bearing mice.

DISCUSSION/CONCLUSION

Histone methylation is one of the major histone modifications that plays a critical role in regulating gene transcription.[33 34] H3K4me3 is a key histone modification that often selectively localizes to target gene promoters and downstream transcription start sites to activate target gene transcription.[34] In this study, we determined that H3K4me3 deposition is altered at the promoters and downstream transcription start sites in a wide range of genes throughout the entire genome in pancreatic tumor as compared with normal pancreas in vivo. This finding suggests that H3K4me3 might play a broad role in gene transcription regulation in the pancreatic cancer genome and that the H3K4me3 epigenome dysregulation plays a critical role in pancreatic cancer pathogenesis and development. ChIP-Seq and RNA-Seq screening identified the ECM-receptor interaction pathway as a major H3K4me3-regulated pathways in pancreatic tumor. Among the genes in this pathway that are up-regulated in pancreatic tumors as compared with normal pancreas are *Cd44* and one of its ligands *Spp1*, the gene that encode OPN protein. CD44 is expressed on tumor cells, myeloid cells, and T cells.[35–37] OPN is known for its function in direct promotion of tumor growth and progression.[38] Emerging experimental data indicate that OPN also functions in immune suppression through interaction with its receptors on myeloid cells and T cells.[37 39–42] We, therefore, focused on OPN in this study, we determined that both CD44 and OPN are upregulated in mouse pancreatic tumors as compared with the normal pancreas. Furthermore, we determined that H3K4me3 deposition in the *Cd44* and *Spp1* promoter regions are increased in pancreatic tumors in vivo. These findings indicate that H3K4me3 may promote pancreatic tumor growth and progression through activating the OPN-CD44 axis to promote pancreatic cancer immune escape.

Despite the low TMBs in pancreatic cancer, there are low to moderate CTL tumor infiltration in human pancreatic cancer,[9–11] suggesting that human pancreatic cancer is not a completely immunologically 'cold' cancer. On the other hand, PD-L1 is expressed in pancreatic tumor cells in the tumor microenvironment.[10 13 14] Furthermore, ICI immunotherapy efficacy can be improved by combined therapies with other immunotherapeutic agents.[43 44] These observations suggest that other immune checkpoints and immune suppressive mechanisms might compensate PD-L1 function in pancreatic cancer immune escape.

Our findings indicate that OPN is such an immune checkpoint that may compensate PD-L1 function to promote immune escape in pancreatic cancer.

Human OPN is encoded by a single copy gene *SPP1*, but it has at least five splicing variants and three of these alternative variants translate into proteins.[45] Furthermore, these protein isoforms have different functions and may contribute to cancer-specific tumor promotion.[46 47] In addition to binding to CD44 through its CD44 hairpin domain, OPN also binds to its integrin receptors αvβ1, αvβ3, αvβ5, αvβ6, α8β1, α5β1 through its RGD domain, and to α9β1, α4β1, α4β7 through its SVVYGLR domain.[48] These observations suggest that OPN neutralization antibody may be efficient to block OPN function in certain types of cancer,[49] it may not be efficient to block all OPN-receptor interactions in the tumor microenvironment. Because all OPN variants are encoded by a single copy gene, targeting OPN expression is potentially a more effective approach. Our finding indicates that targeting H3K4me3 is effective in repression of OPN expression in pancreatic tumors and MDSCs. WDR5 is essential for all histone methyltransferase activity in catalyzing H3K4me3.[30] WDR5-47, WDR5-0102, and Cpd23 were originally designed and developed for leukemia therapy.[27 30 50] We determined in this study that these WDR5 inhibitors have different cytotoxicity to pancreatic tumor cells and MDSCs. WDR5-47 is relatively less cytotoxic but is effective in repressing OPN expression to suppress pancreatic tumor growth in vivo. Furthermore, inhibition of WDR5 also significantly improved the efficacy of anti-PD-1 immunotherapy in suppression of pancreatic tumor growth in vivo. However, knocking out OPN significantly suppressed pancreatic tumor growth, knocking out OPN is less effective than inhibiting the WDR5-H3K4me3-OPN axis in augmentation of anti-PD-1 efficacy. This phenomenon indicates that, in addition to OPN, the WDR5-H3K4me3 pathway likely also regulates other immune checkpoints and immune suppressors. Further studies are needed to identify these potential immune checkpoints and immune suppressors.

One limitation of this study is the phenomenon that the mouse pancreatic carcinomas used in this study are responsive to anti-PD-1 immunotherapy, whereas human pancreatic cancer does not respond to anti-PD-1 immunotherapy. The findings made in these mouse tumor models may not be fully translational. Further validation of our findings in a more human pancreatic cancer relevant mouse tumor model, such as the human pancreatic cancer patient-derived xenograft humanized NSG mouse model, is needed before translating WDR5 inhibition as an enhancer of ICI immunotherapy in human pancreatic cancer patients.

Author affiliations
[1]School of Life Sciences, Tianjin University, Tianjin, China
[2]Department of Biochemistry and Molecular Biology, Nanchang University, Nanchang, China
[3]Department of Biochemistry and Molecular Biology, Medical College of Georgia, Augusta, Georgia, USA
[4]Georgia Cancer Center, Medical College of Georgia, Augusta, Georgia, USA
[5]Charlie Norwood VA Medical Center, Augusta, Georgia, USA
[6]Department of Population Health Science, Medical College of Georgia, Augusta, Georgia, USA

Acknowledgements We thank Dr. Roni Bollag at Georgia Cancer Center for providing human serum specimens. This work was supported by the National Cancer Institute grants R01CA227433 and R01CA133085 (to KL), F30CA236436-01 (to JDK), F31CA257212-01 (to ADM), National Natural Science Foundation of China grant 81802858 (to CL), and US Department of Veterans Affairs Award CX001364 (to KL).

Contributors CL, ZL, JDK, DY, ADM, DP and TA performed experiments, collected data, and analyzed data. JLW performed statistical analysis. CL, JLW, HS and KL designed the studies and wrote the manuscript.

Competing interests No, there are no competing interests.

Patient consent for publication Not required.

Ethics approval All studies with human specimens were approved by Augusta University Institutional Review Board (Approval # 9 33 148–1). All studies with mice were approved by Augusta University Institutional Animal Care and Use Committee (Protocol # 2008–0162).

Provenance and peer review Not commissioned; externally peer reviewed.

Data availability statement Data are available in a public, open access repository. NA.

ORCID iD
Kebin Liu http://orcid.org/0000-0003-1965-7240

REFERENCES

1 Robert C. A decade of immune-checkpoint inhibitors in cancer therapy. *Nat Commun* 2020;11:3801.
2 Royal RE, Levy C, Turner K, *et al*. Phase 2 trial of single agent ipilimumab (anti-CTLA-4) for locally advanced or metastatic pancreatic adenocarcinoma. *J Immunother* 2010;33:828–33.
3 O'Reilly EM, Oh D-Y, Dhani N, *et al*. Durvalumab with or without tremelimumab for patients with metastatic pancreatic ductal adenocarcinoma: a phase 2 randomized clinical trial. *JAMA Oncol* 2019;5:1431–8.
4 O'Hara MH, O'Reilly EM, Varadhachary G, *et al*. Cd40 agonistic monoclonal antibody APX005M (sotigalimab) and chemotherapy, with or without nivolumab, for the treatment of metastatic pancreatic adenocarcinoma: an open-label, multicentre, phase 1B study. *Lancet Oncol* 2021;22:118–31.
5 Le DT, Durham JN, Smith KN, *et al*. Mismatch repair deficiency predicts response of solid tumors to PD-1 blockade. *Science* 2017;357:409–13.
6 Principe DR, Korc M, Kamath SD. Trials and tribulations of pancreatic cancer immunotherapy. *Cancer Lett* 2021;504:1–14.
7 Hu ZI, Shia J, Stadler ZK, *et al*. Evaluating mismatch repair deficiency in pancreatic adenocarcinoma: challenges and recommendations. *Clin Cancer Res* 2018;24:1326–36.
8 Waddell N, Pajic M, Patch A-M, *et al*. Whole genomes redefine the mutational landscape of pancreatic cancer. *Nature* 2015;518:495–501.

9 Schmitz-Winnenthal FH, Volk C, Z'graggen K, *et al*. High frequencies of functional tumor-reactive T cells in bone marrow and blood of pancreatic cancer patients. *Cancer Res* 2005;65:10079–87.
10 Lu C, Talukder A, Savage NM, *et al*. JAK-STAT-mediated chronic inflammation impairs cytotoxic T lymphocyte activation to decrease anti-PD-1 immunotherapy efficacy in pancreatic cancer. *Oncoimmunology* 2017;6:e1291106.
11 Blando J, Sharma A, Higa MG, *et al*. Comparison of immune infiltrates in melanoma and pancreatic cancer highlights vista as a potential target in pancreatic cancer. *Proc Natl Acad Sci U S A* 2019;116:1692–7.
12 Ware MB, El-Rayes BF, Lesinski GB. Mirage or long-awaited OASIS: reinvigorating T-cell responses in pancreatic cancer. *J Immunother Cancer* 2020;8:e001100.
13 Gao H-L, Liu L, Qi Z-H, *et al*. The clinicopathological and prognostic significance of PD-L1 expression in pancreatic cancer: a meta-analysis. *Hepatobiliary Pancreat Dis Int* 2018;17:95–100.
14 Lu C, Paschall AV, Shi H, *et al*. The MLL1-H3K4me3 Axis-Mediated PD-L1 expression and pancreatic cancer immune evasion. *J Natl Cancer Inst* 2017;109:djw283.
15 Mace TA, Shakya R, Pitarresi JR, *et al*. Il-6 and PD-L1 antibody blockade combination therapy reduces tumour progression in murine models of pancreatic cancer. *Gut* 2018;67:320–32.
16 Zhang Y, Ware MB, Zaidi MY, *et al*. Heat shock protein-90 inhibition alters activation of pancreatic stellate cells and enhances the efficacy of PD-1 blockade in pancreatic cancer. *Mol Cancer Ther* 2021;20:150–60.
17 Ho WJ, Jaffee EM, Zheng L. The tumour microenvironment in pancreatic cancer - clinical challenges and opportunities. *Nat Rev Clin Oncol* 2020;17:527–40.
18 Pauken KE, Sammons MA, Odorizzi PM, *et al*. Epigenetic stability of exhausted T cells limits durability of reinvigoration by PD-1 blockade. *Science* 2016;354:1160–5.
19 Nephew KP. Turning up the heat on the pancreatic tumor microenvironment by epigenetic priming. *Cancer Res* 2020;80:4610–1.
20 Lomberk G, Dusetti N, Iovanna J, *et al*. Emerging epigenomic landscapes of pancreatic cancer in the era of precision medicine. *Nat Commun* 2019;10:3875.
21 Gonda TA, Fang J, Salas M, *et al*. A DNA hypomethylating drug alters the tumor microenvironment and improves the effectiveness of immune checkpoint inhibitors in a mouse model of pancreatic cancer. *Cancer Res* 2020;80:4754–67.
22 Lu C, Yang D, Sabbatini ME, *et al*. Contrasting roles of H3K4me3 and H3K9me3 in regulation of apoptosis and gemcitabine resistance in human pancreatic cancer cells. *BMC Cancer* 2018;18:149.
23 Zheng L. Pd-L1 expression in pancreatic cancer. *J Natl Cancer Inst* 2017;109:djw304.
24 Torres MP, Rachagani S, Souchek JJ, *et al*. Novel pancreatic cancer cell lines derived from genetically engineered mouse models of spontaneous pancreatic adenocarcinoma: applications in diagnosis and therapy. *PLoS One* 2013;8:e80580.
25 Wang Y, Zhang Y, Yang J, *et al*. Genomic sequencing of key genes in mouse pancreatic cancer cells. *Curr Mol Med* 2012;12:331–41.
26 Zhu H, Klement JD, Lu C, *et al*. Asah2 represses the p53-Hmox1 axis to protect myeloid-derived suppressor cells from ferroptosis. *J Immunol* 2021;206:1395–404.
27 Bolshan Y, Getlik M, Kuznetsova E, *et al*. Synthesis, optimization, and evaluation of novel small molecules as antagonists of WDR5-MLL interaction. *ACS Med Chem Lett* 2013;4:353–7.
28 Li D-D, Chen W-L, Xu X-L, DD L, XL X, *et al*. Structure-Based design and synthesis of small molecular inhibitors disturbing the interaction of MLL1-WDR5. *Eur J Med Chem* 2016;118:1–8.
29 Ran FA, Hsu PD, Wright J, *et al*. Genome engineering using the CRISPR-Cas9 system. *Nat Protoc* 2013;8:2281–308.
30 Li Y, Han J, Zhang Y, *et al*. Structural basis for activity regulation of MLL family methyltransferases. *Nature* 2016;530:447–52.
31 Reynoird N, Mazur PK, Stellfeld T, *et al*. Coordination of stress signals by the lysine methyltransferase SMYD2 promotes pancreatic cancer. *Genes Dev* 2016;30:772–85.
32 Kägi D, Vignaux F, Ledermann B, *et al*. Fas and perforin pathways as major mechanisms of T cell-mediated cytotoxicity. *Science* 1994;265:528–30.
33 Zong X, Wang W, Ozes A, *et al*. Ezh2-Mediated downregulation of the tumor suppressor DAB2IP maintains ovarian cancer stem cells. *Cancer Res* 2020;80:4371–85.
34 Liu X, Wang C, Liu W, *et al*. Distinct features of H3K4me3 and H3K27me3 chromatin domains in pre-implantation embryos. *Nature* 2016;537:558–62.
35 Zhang S, Balch C, Chan MW, *et al*. Identification and characterization of ovarian cancer-initiating cells from primary human tumors. *Cancer Res* 2008;68:4311–20.
36 Rao G, Wang H, Li B, *et al*. Reciprocal interactions between tumor-associated macrophages and CD44-positive cancer cells via osteopontin/CD44 promote tumorigenicity in colorectal cancer. *Clin Cancer Res* 2013;19:785–97.
37 Klement JD, Paschall AV, Redd PS, *et al*. An osteopontin/CD44 immune checkpoint controls CD8+ T cell activation and tumor immune evasion. *J Clin Invest* 2018;128:5549–60.
38 Chakraborty G, Jain S, Kundu GC. Osteopontin promotes vascular endothelial growth factor-dependent breast tumor growth and angiogenesis via autocrine and paracrine mechanisms. *Cancer Res* 2008;68:152–61.
39 Chiodoni C, Sangaletti S, Tripodo C, *et al*. The Ins and outs of osteopontin. *Oncoimmunology* 2015;4:e978711.
40 Cheng J, Huo D-H, Kuang D-M, *et al*. Human macrophages promote the motility and invasiveness of osteopontin-knockdown tumor cells. *Cancer Res* 2007;67:5141–7.
41 Sangaletti S, Tripodo C, Sandri S, *et al*. Osteopontin shapes immunosuppression in the metastatic niche. *Cancer Res* 2014;74:4706–19.
42 Wei J, Marisetty A, Schrand B, *et al*. Osteopontin mediates glioblastoma-associated macrophage infiltration and is a potential therapeutic target. *J Clin Invest* 2019;129:137–49.
43 Kim VM, Blair AB, Lauer P, *et al*. Anti-Pancreatic tumor efficacy of a Listeria-based, annexin A2-targeting immunotherapy in combination with anti-PD-1 antibodies. *J Immunother Cancer* 2019;7:132.
44 Muth ST, Saung MT, Blair AB, *et al*. Cd137 agonist-based combination immunotherapy enhances activated, effector memory T cells and prolongs survival in pancreatic adenocarcinoma. *Cancer Lett* 2021;499:99–108.
45 Briones-Orta MA, Avendaño-Vázquez SE, Aparicio-Bautista DI, *et al*. Osteopontin splice variants and polymorphisms in cancer progression and prognosis. *Biochimica et Biophysica Acta (BBA) - Reviews on Cancer* 2017;1868:93–108.
46 He B, Mirza M, Weber GF. An osteopontin splice variant induces anchorage independence in human breast cancer cells. *Oncogene* 2006;25:2192–202.
47 Mirza M, Shaughnessy E, Hurley JK, *et al*. Osteopontin-C is a selective marker of breast cancer. *Int J Cancer* 2008;122:889–97.
48 Kahles F, Findeisen HM, Bruemmer D. Osteopontin: a novel regulator at the cross roads of inflammation, obesity and diabetes. *Mol Metab* 2014;3:384–93.
49 Klement JD, Poschel DB, Lu C, *et al*. Osteopontin blockade immunotherapy increases cytotoxic T lymphocyte lytic activity and suppresses colon tumor progression. *Cancers* 2021;13:1006.
50 Li D-D, Chen W-L, Wang Z-H, *et al*. High-affinity small molecular blockers of mixed lineage leukemia 1 (MLL1)-WDR5 interaction inhibit MLL1 complex H3K4 methyltransferase activity. *Eur J Med Chem* 2016;124:480–9.

Supplemental Data

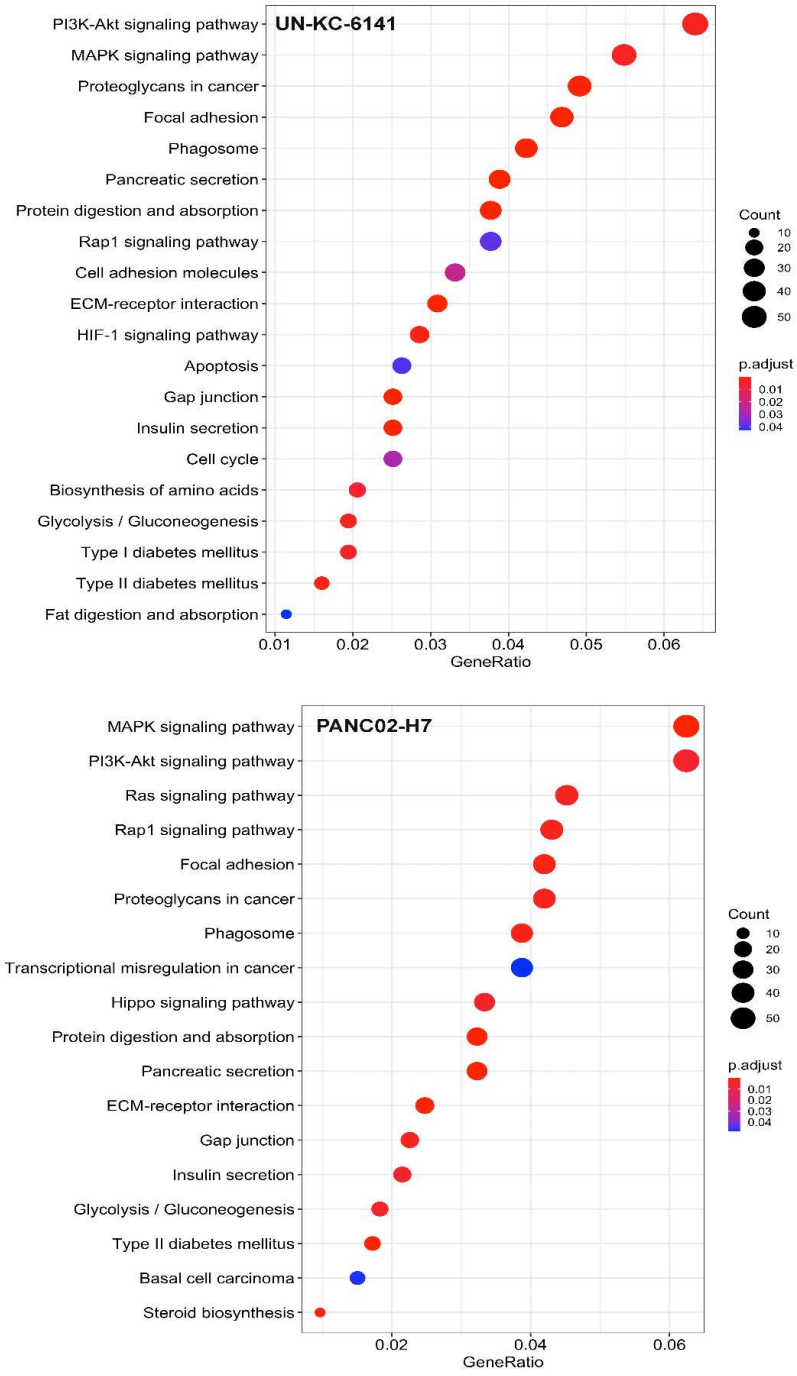

Figure S1. KEGG pathway enrichment in pancreatic carcinoma in vivo. The differentially expressed genes between normal pancreas and the two orthotopic pancreatic tumors were analyzed for pathway enrichment using R package clusterProfiler. Benjamini-Hochberg (BH)-adjusted p-value <0.05) was used as cutoff value.

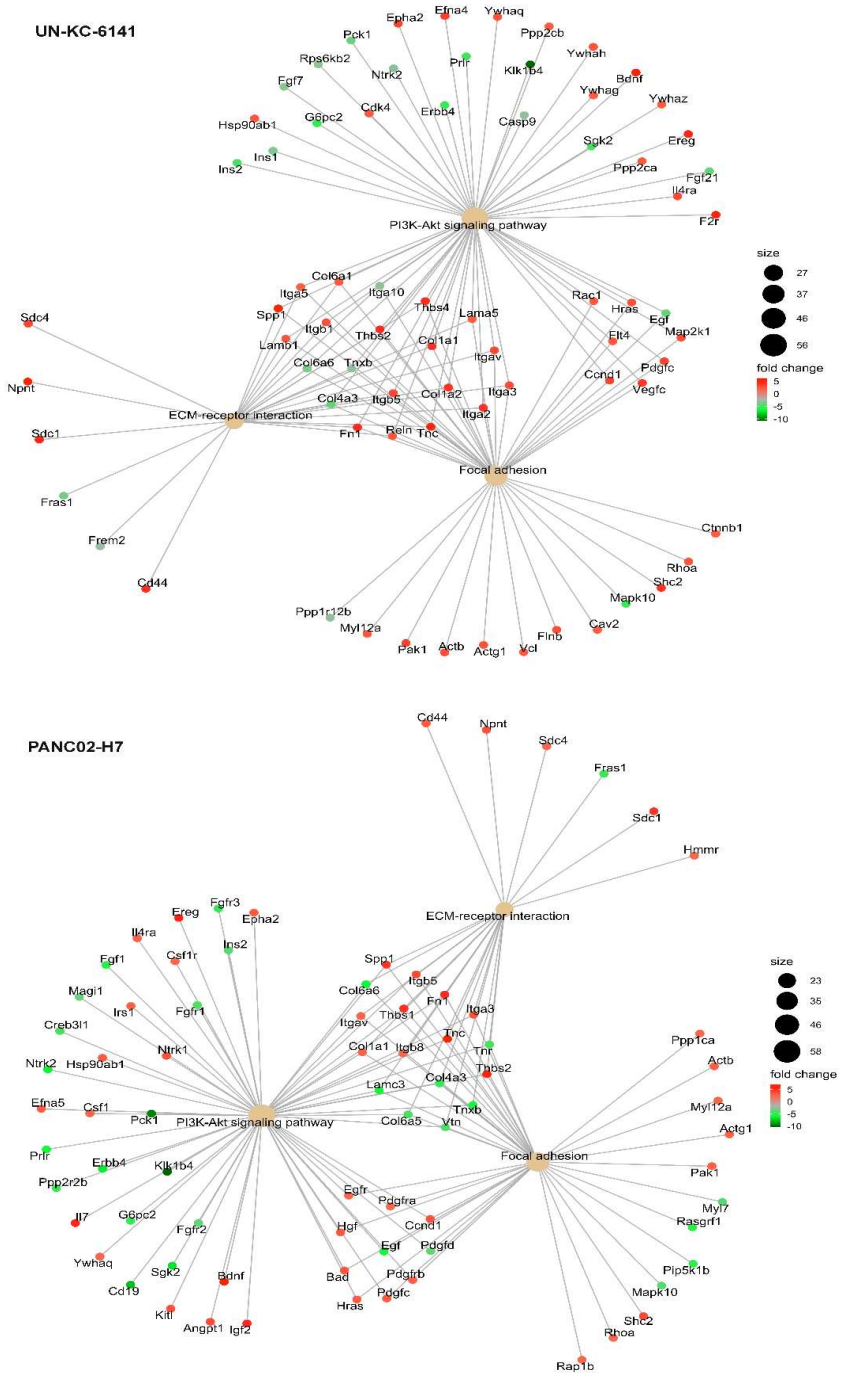

Figure S2. Differentially expressed genes in KEGG pathway. The differentially expressed genes between normal pancreas and the two orthotopic pancreatic tumors in the three indicated pathways are shown in cnet plots generated by clusterProfiler.

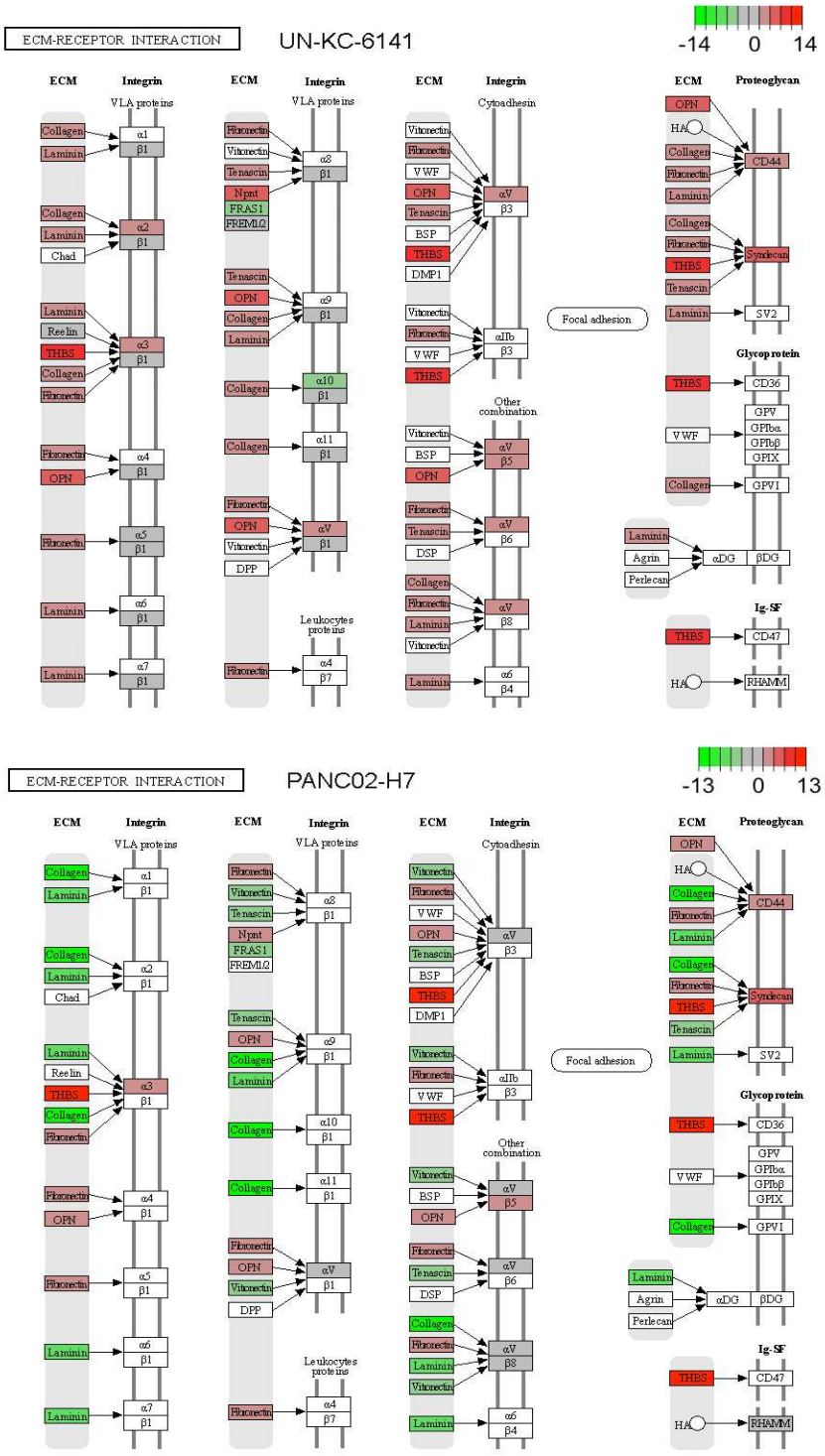

Figure S3. ECM-receptor interaction map. The differentially expressed genes were mapped to their respective ligands or receptors using R package pathview. Red color indicates up-regulated genes in tumors and green color indicates down-regulated genes in tumors.

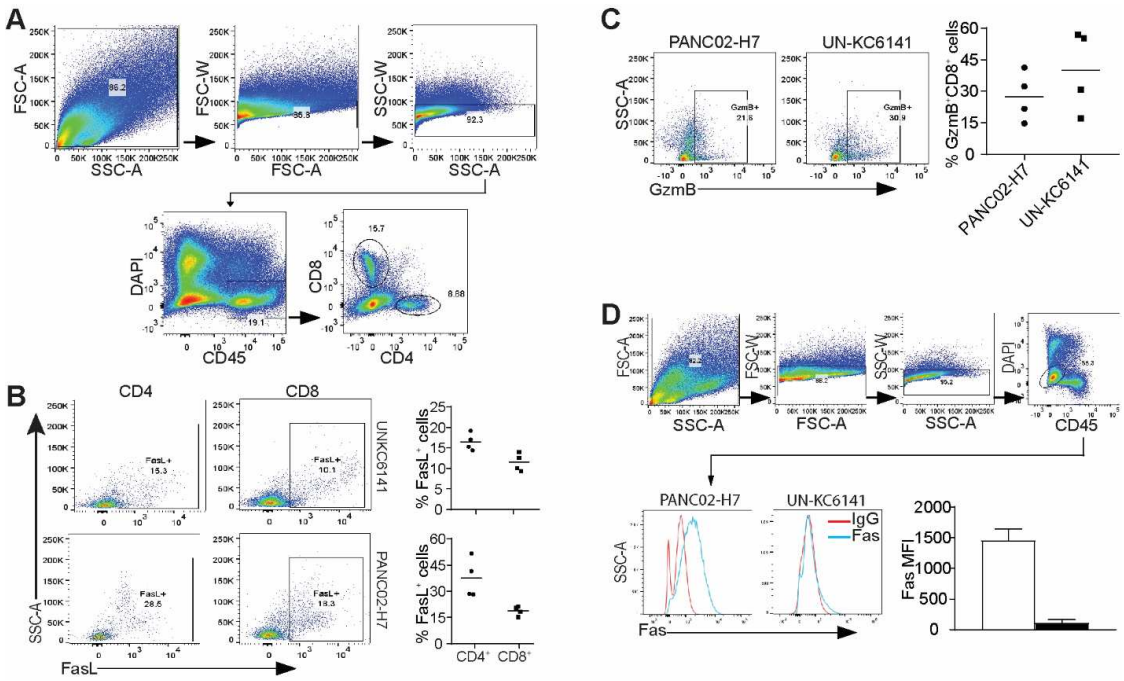

Figure S4. T cell effector and tumor death receptor expression in pancreatic carcinoma. **A**. The orthotopic UN-KC-6141 and PANC02-H7 tumors were collected from tumor-bearing mice and processed for analysis of tumor cells and tumor-infiltrating immune cells. Shwon is gating strategy. **B**. FasL expression in T cells as gated in A was analyzed by flow cytometry. The % FasL$^+$ cells were quantified and presented at the right. **C**. Gzmb expression in tumor-infiltrating CD8$^+$ T cells was analyzed and quantified. **D**. Live tumor cells were gated and and analyzed for Fas expression level in the two tumors. The Fas MFI is quantified at the right panel.

Table S1. Normal human pancreas

Patient	Tissue	Age	Race	Sex	Patient diagonosis	Treatment prior to tissue resection
15-01-A072d-1	Normal Pancreas	40	Black	Female	Cholangiocarcinoma	None
15-01-A076c-1	Normal Pancreas	62	White	Female	Neuroendocrine tumor	None
15-02-A084a-b	Normal Pancreas	22	Black	Male	Adrenal cortical carcinoma	None
15-03-A038c-1	Normal Pancreas	73	White	Male	Adenocarcinoma of pancreas	None
15-05-A033d-1	Normal Pancreas	63	Black	Male	Adenocarcinoma of pancreas	None

Table S2. Human pancreatic tumor tissues

Patient	Diagnosis of Samples	Age	Race	Sex	Treatment prior to tumor resection
15-01-A016c-1	Adenocarcinoma of pancreas	70	White	Female	None
15-02-A095i-1	Adenocarcinoma of pancreas	74	White	Male	None
15-05-A070a-1	Adenocarcinoma of pancreas	69	White	Female	None
15-05-A085e	Adenocarcinoma of pancreas	70	White	Female	None
15-08-A037d-1	Adenocarcinoma of pancreas	53	White	Male	None

Table S3. Patient survival and OPN expression level

Patient	Days	Status	OPN Expression	Cutoff
TCGA-3A-A9IR	1542	Alive	29.95	Low
TCGA-FB-AAPP	485	Dead	202.4	Low
TCGA-3A-A9IS	998	Alive	237.62	Low
TCGA-3A-A9IN	2084	Alive	373.56	Low
TCGA-US-A776	1216	Alive	376.78	Low
TCGA-FB-AAPU	381	Dead	553.8	Low
TCGA-2J-AABA	607	Dead	1021.45	Low
TCGA-3A-A9IV	1103	Alive	1071.98	Low
TCGA-HZ-7289	661	Dead	1106.12	Low
TCGA-2L-AAQE	684	Dead	1178.87	Low
TCGA-3A-A9IO	1942	Alive	1196.95	Low
TCGA-3A-A9IJ	1854	Alive	1211.86	Low
TCGA-Z5-AAPL	467	Alive	1747.58	Low
TCGA-3A-A9I7	1323	Alive	1780.22	Low
TCGA-FB-AAQ0	473	Dead	1982.29	Low
TCGA-HZ-A49I	308	Dead	1987.07	Low
TCGA-2J-AAB8	80	Alive	2047.47	Low
TCGA-HZ-8637	517	Dead	2324.37	Low
TCGA-S4-A8RM	737	Alive	2338.05	Low
TCGA-3A-A9IL	2741	Alive	2357.64	Low
TCGA-IB-AAUR	338	Alive	2394.05	Low
TCGA-XD-AAUH	395	Alive	2513.79	Low
TCGA-LB-A7SX	393	Dead	2564.77	Low
TCGA-3E-AAAZ	2182	Dead	2703.07	Low
TCGA-IB-AAUP	431	Alive	2737.21	Low
TCGA-XN-A8T5	720	Alive	2892.13	Low
TCGA-IB-A5ST	635	Alive	2998.69	Low
TCGA-Q3-AA2A	95	Alive	3041.82	Low
TCGA-HZ-A4BH	194	Alive	3250.78	Low
TCGA-FB-A7DR	353	Dead	3271.69	Low
TCGA-2J-AABP	463	Alive	3283.53	Low
TCGA-F2-6879	334	Dead	3904.59	Low
TCGA-HZ-A4BK	657	Alive	4019.77	Low
TCGA-2J-AABI	969	Alive	4062.77	Low
TCGA-HZ-8519	454	Alive	4161.49	Low
TCGA-US-A77G	12	Dead	4324.97	Low
TCGA-HZ-7925	614	Dead	4511.45	Low
TCGA-IB-A7M4	483	Alive	4636.06	Low
TCGA-YY-A8LH	2016	Alive	4688.35	Low
TCGA-L1-A7W4	278	Dead	4776.67	Low
TCGA-XD-AAUG	420	Alive	4908.11	Low
TCGA-IB-7897	486	Dead	5229.49	Low
TCGA-HV-A7OL	252	Alive	5260.63	Low
TCGA-2J-AABU	277	Dead	5587.34	Low
TCGA-IB-7888	1332	Dead	5741.88	Low
TCGA-HV-A5A6	2036	Dead	5768.74	Low
TCGA-HZ-7924	840	Alive	5809.23	Low
TCGA-HV-AA8X	532	Dead	6011.24	Low
TCGA-FB-AAQ2	153	Dead	6094.93	Low
TCGA-HZ-A8P1	7	Alive	6179.04	Low
TCGA-FB-AAQ6	244	Dead	6257.28	Low
TCGA-H8-A6C1	671	Alive	6317.89	Low
TCGA-IB-7647	666	Dead	6349.45	Low
TCGA-YH-A8SY	388	Alive	6507.59	Low
TCGA-2J-AABO	440	Alive	6709.94	Low
TCGA-HZ-A49H	491	Alive	7039.62	Low
TCGA-HZ-8001	706	Alive	7123.93	Low
TCGA-IB-7887	110	Dead	7208.2	Low
TCGA-M8-A5N4	584	Alive	7436.53	Low
TCGA-FB-A5VM	498	Dead	7870.11	Low
TCGA-HZ-A77Q	33	Alive	7876.62	Low

TCGA-HV-A5A4	232	Alive	7928	Low
TCGA-IB-AAUV	404	Alive	8199.59	Low
TCGA-HZ-A77P	330	Alive	8412.58	Low
TCGA-IB-7645	1502	Dead	8462.79	Low
TCGA-IB-7886	123	Dead	8649.31	Low
TCGA-F2-A8YN	517	Alive	8732.08	Low
TCGA-IB-A5SP	482	Alive	9206.7	Low
TCGA-IB-7644	394	Dead	9437.12	Low
TCGA-3A-A9IB	224	Dead	9727.7	Low
TCGA-IB-AAUM	8	Alive	9736.92	High
TCGA-2J-AAB1	66	Dead	9841.95	High
TCGA-Q3-A5QY	416	Alive	9908.15	High
TCGA-IB-8127	522	Alive	10156.83	High
TCGA-HZ-7920	236	Dead	10413.23	High
TCGA-OE-A75W	267	Dead	11076.46	High
TCGA-HZ-8317	378	Dead	11114.06	High
TCGA-HZ-A9TJ	603	Alive	11400.16	High
TCGA-US-A779	511	Dead	12075.49	High
TCGA-2L-AAQA	143	Dead	12522.02	High
TCGA-2J-AABT	319	Alive	12588.24	High
TCGA-2J-AABE	676	Alive	12628.33	High
TCGA-2J-AAB6	293	Dead	12734.5	High
TCGA-3A-A9IC	738	Dead	12843.46	High
TCGA-F2-6880	295	Alive	12877.57	High
TCGA-F2-A44G	233	Dead	13081.68	High
TCGA-IB-7654	476	Dead	13128.45	High
TCGA-FB-A545	732	Dead	13270.25	High
TCGA-2L-AAQJ	394	Dead	13295.54	High
TCGA-XD-AAUL	498	Alive	13317.26	High
TCGA-IB-7885	1257	Alive	13350.34	High
TCGA-IB-A5SQ	219	Dead	13569.78	High
TCGA-HZ-8315	299	Dead	14132.15	High
TCGA-IB-8126	462	Alive	14370.9	High
TCGA-H6-8124	392	Alive	14461.94	High
TCGA-HZ-7919	593	Dead	14492.59	High
TCGA-RB-A7B8	466	Dead	15006.57	High
TCGA-IB-AAUN	144	Dead	15283.87	High
TCGA-IB-AAUS	225	Alive	15290.54	High
TCGA-S4-A8RP	702	Dead	15678.67	High
TCGA-HZ-8003	596	Dead	15751.44	High
TCGA-IB-A5SO	365	Dead	15827.59	High
TCGA-FB-A78T	375	Dead	16106.12	High
TCGA-IB-AAUO	239	Dead	16143.88	High
TCGA-2J-AABH	1287	Alive	17129.36	High
TCGA-2J-AABF	691	Dead	17151.77	High
TCGA-IB-A7LX	250	Dead	17863.21	High
TCGA-FB-AAPZ	716	Alive	18144.1	High
TCGA-HZ-7922	4	Alive	18801.71	High
TCGA-F2-A44H	586	Alive	19079.42	High
TCGA-3A-A9IX	1037	Alive	19274.32	High
TCGA-HZ-7926	518	Dead	19388.49	High
TCGA-YB-A89D	350	Alive	19501.03	High
TCGA-FB-AAPS	228	Alive	20690.34	High
TCGA-US-A774	695	Dead	20886.74	High
TCGA-PZ-A5RE	470	Dead	21074.61	High
TCGA-S4-A8RO	525	Alive	21572.98	High
TCGA-3A-A9J0	743	Alive	21613.94	High
TCGA-US-A77E	430	Dead	21795.63	High
TCGA-IB-AAUU	245	Alive	21932.25	High
TCGA-XD-AAUI	366	Dead	22054.98	High
TCGA-IB-7646	145	Dead	22161.93	High
TCGA-HV-A5A3	128	Dead	22572.62	High
TCGA-RB-AA9M	286	Alive	23967.81	High

TCGA-3A-A9IZ	308	Dead	24070.63	High
TCGA-HZ-7923	314	Alive	24675.28	High
TCGA-3A-A9IH	1021	Alive	24914.14	High
TCGA-XN-A8T3	951	Alive	24935.13	High
TCGA-LB-A8F3	379	Alive	25001.02	High
TCGA-FB-AAPY	1059	Dead	25192.31	High
TCGA-3A-A9IU	458	Dead	25219.68	High
TCGA-HZ-A77O	160	Dead	25311.31	High
TCGA-FB-A4P6	767	Alive	25506.81	High
TCGA-H6-A45N	421	Dead	25839.44	High
TCGA-US-A77J	568	Dead	26733.86	High
TCGA-IB-7889	481	Dead	26952.62	High
TCGA-2L-AAQL	292	Dead	27025.79	High
TCGA-3E-AAAY	2285	Alive	27438.32	High
TCGA-IB-A5SS	460	Dead	27680.8	High
TCGA-HZ-7918	969	Alive	27937.01	High
TCGA-2J-AABK	484	Alive	28105.33	High
TCGA-F2-7273	592	Dead	28580.44	High
TCGA-FB-A4P5	179	Dead	29006.72	High
TCGA-2L-AAQM	1383	Alive	29088.43	High
TCGA-HZ-8636	545	Dead	29496.46	High
TCGA-IB-7651	603	Dead	29782.79	High
TCGA-IB-AAUQ	183	Dead	31128.83	High
TCGA-HZ-8002	366	Dead	32323.35	High
TCGA-F2-A7TX	95	Dead	33146	High
TCGA-FB-AAPQ	1130	Dead	33150.55	High
TCGA-IB-7652	1116	Alive	33716.41	High
TCGA-RL-AAAS	9	Alive	33788.32	High
TCGA-2J-AABR	438	Alive	35384.04	High
TCGA-IB-7893	117	Dead	35603.45	High
TCGA-2L-AAQI	103	Dead	39661.07	High
TCGA-F2-7276	216	Dead	39898.19	High
TCGA-IB-AAUW	230	Dead	40794.34	High
TCGA-IB-A6UG	41	Dead	42115.01	High
TCGA-3A-A9I9	634	Dead	42269.69	High
TCGA-IB-7891	913	Dead	44550.66	High
TCGA-HZ-8005	120	Dead	44715.83	High
TCGA-2J-AABV	652	Dead	46651.97	High
TCGA-LB-A9Q5	313	Dead	46887.42	High
TCGA-FB-AAQ3	31	Dead	47218.68	High
TCGA-2J-AAB9	627	Dead	47747.05	High
TCGA-IB-7890	598	Dead	49693.05	High
TCGA-IB-A6UF	666	Alive	53108.57	High
TCGA-2J-AAB4	729	Alive	54838.38	High
TCGA-IB-7649	467	Dead	61621.51	High
TCGA-IB-AAUT	287	Alive	63261.96	High
TCGA-HZ-A49G	660	Alive	67481.4	High
TCGA-FB-AAQ1	123	Dead	68175.37	High
TCGA-HV-AA8V	920	Alive	70061.59	High
TCGA-HV-A5A5	289	Alive	73456.38	High
TCGA-3A-A9I5	1794	Alive	96867.35	High

Table S4. PCR primers

mSPP1-F1	GCCTGTTTGGCATTGCCTCCTC
mSPP1-B1	CACAGCATTCTGTGGCGCAAGG
mCD44-F	ACTCAAGTGCGAACCAGGACAG
mCD44-B	GCTTTTTCTTCTGCCCACACC
mSpp1-ChIP-1F	GAGGAAACCAGCCAAGGTAAGC
mSpp1-ChIP-1B	CAAAAAGACCAGAACAGCACGAG
mSpp1-ChIP-2F	AGGGTCTGAAAGTTCTGCCGAG
mSpp1-ChIP-2B	GGGGATGAAAGGTATGGATTCTCC
mSpp1-ChIP3-F	AGCAGGGTTTGGCAAGTAGCAC
mSpp1-ChIP3-B	TCCCGAAATGGAGAACACAGGC
mSpp1-ChIP-4F	TTAACCCCAGTGGCTACACG
mSpp1-ChIP-4B	TCATGTTGAAGTCCCCTTAAAGTAG

Table S5. Flow cytometry antibodies

Antibody	Source	Clone	Cat Number	Application
PE-Cy7 anti-mouse CD45.2	Biolegend	104	109830	Flow Cytometry
FITC anti-mouse CD4	Biolegend	GK1.5	100406	Flow Cytometry
PerCP anti-mouse CD8	Biolegend	53-6.7	100732	Flow Cytometry
APC anti-mouse PD-1	Biolegend	29F.1A12	135210	Flow Cytometry
PE anti-mouse FasL	Biolegend	Kay-10	106805	Flow Cytometry
FITC anti-human/mouse CD11b	Biolegend	M1/70	101206	Flow Cytometry
PerCP anti-mouse Gr1	Biolegend	RB6-8C5	108426	Flow Cytometry
APC anti-mouse PD-L1	Biolegend	10F.9G2	124312	Flow Cytometry
AF700 anti-mouse Ly6G	Biolegend	1A8	127622	Flow Cytometry
PerCP anti-mouse Ly6C	Biolegend	HK1.4	128028	Flow Cytometry
PE-Cy7 anti-mouse F4/80	Biolegend	BM8	123114	Flow Cytometry
AF700 anti-mouse CD206	Biolegend	C068C2	141734	Flow Cytometry
FITC anti-mouse Fas	BD Pharmingen	Jo2	554257	Flow Cytometry
PE anti-mouse OPN	R&D Systems	N/A	IC808P	Flow Cytometry
Pacific Blue anti-human/mouse GzmB	Biolegend	GB11	515408	Flow Cytometry
FITC mouse IgG	Biolegend	Poly4060	406001	Flow Cytometry
APC Armenian Hamster IgG	Biolegend	HTK888	400912	Flow Cytometry

Table S6: Two-factor ANOVA results of WDR5-47 and anti-PD-1 immunotherapy on tumor weight and size

Outcome	Effect in Model	Level of WDR5-047	Level of anti-PD-1	Mean	SD	F-value	*p*-value
Tumor Weight	WDR5-047 status	WDR5-047		0.2256	0.1051	75.88	<0.0001
		Control		0.5988	0.2473		
	anti-PD-1 status		anti-PD-1	0.2788	0.1541	38.82	<0.0001
			Control	0.5456	02911		
	WDR5-047 Status x anti-PD-1 status	WDR5-047	anti-PD-1	0.1488	0.0380	6.97	0.0134
			Control	0.3025	0.0935		
		Control	anti-PD-1	0.4088	0.1040		
			Control	0.7888	0.1942		
Tumor Size	WDR5-047 Status	WDR5-047		213.4229	123.4092	58.32	<0.0001
		Control		851.5887	506.8368		
	anti-PD-1 status		anti-PD-1	300.7270	194.1639	30.77	<0.0001
			Control	764.2846	580.5266		
	WDR5-047 Status x anti-PD-1 status	WDR5-047	anti-PD-1	139.5968	31.4927	14.29	0.0008
			Control	287.2491	138.5125		
		Control	anti-PD-1	461.8573	143.0007		
			Control	1241.3201	427.5947		

Table S7 Two-factor ANOVA results of WT (Scramble)/*Spp1* KO and anti-PD-1 immunotherapy on tumor weight and size.

Outcome	Effect in Model	Level of Cell Type	Level of anti-PD-1	Mean	SD	F-value	*p*-value
Tumor Weight	Cell type	Scramble		0.29	0.14	27.01	<0.0001
		Spp1 KO		0.14	0.04		
	anti-PD-1 status		anti-PD-1	0.16	0.05	14.20	0.0011
			IgG	0.25	0.14		
	Cell type x anti-PD-1 status	Scramble	anti-PD-1	0.21	0.02	5.28	0.0319
			IgG	0.38	0.15		
		Spp1 KO	anti-PD-1	0.12	0.03		
			IgG	0.17	0.04		
Tumor Size	Cell type	Scramble		416.76	170.39	60.07	<0.0001
		Spp1 KO		147.77	59.95		
	anti-PD-1 status		anti-PD-1	180.43	125.87	21.53	0.0001
			IgG	322.13	190.77		
	Cell type x anti-PD-1 status	Scramble	anti-PD-1	305.13	97.94	2.59	0.1227
			IgG	522.40	161.94		
		Spp1 KO	anti-PD-1	91.54	21.79		
			IgG	196.96	29.20		